OPTIMIZATION OF ELECTRIC VEHICLES WIRELESS CHARGING

by

Abdalla Gesrou

A Thesis Presented to the Faculty of the
American University of Sharjah
College of Engineering
in Partial Fulfillment
of the Requirements
for the Degree of

Master of Science in
Mechatronics Engineering

Sharjah, United Arab Emirates

December 2019

Approval Signatures

We, the undersigned, approve the Master's Thesis of Abdalla Gesrou

Thesis Title: Optimization of Electric Vehicles Wireless Charging.

Signature **Date of Signature** (dd/mm/yyyy)

_____ _____

Dr. Ahmed Osman-Ahmed
Professor, Department of Electrical Engineering
Thesis Advisor

_____ _____

Dr. Shayok Mukhopadhyay
Assistant Professor, Department of Electrical Engineering
Thesis Co-Advisor

_____ _____

Dr. Lotfi Romdhane
Professor, Department of Mechanical Engineering
Thesis Committee Member

_____ _____

Dr. Mostafa Farouk Shaaban
Assistant Professor, Department of Electrical Engineering
Thesis Committee Member

_____ _____

Dr. Mohammad Jaradat
Professor, Department of Mechanical Engineering
Director of Mechatronics graduate program

_____ _____

Dr. Lotfi Romdhane
Associate Dean for Graduate Affairs and Research, College of Engineering

_____ _____

Dr. Naif Darwish
Acting Dean, College of Engineering

_____ _____

Dr. Mohamed El-Tarhuni
Vice Provost for Graduate Studies

Acknowledgement

I would like to take the chance to deeply thank my advisors Dr. Ahmed Osman-Ahmed and Dr. Shayok Mukhopadhyay for generously providing me with guidance and support throughout my research stages. I am greatly thankful for their time, efforts, suggestions, and worthy discussions.

Moreover, I would like to express my gratefulness for the American University of Sharjah for providing me with the Graduate Teaching Assistantship throughout the two years of the Mechatronics master's program.

I would also like to thank the Mechatronics, Electrical, and Mechanical departments' professors who taught me the master level courses with beneficial teaching methods and advanced skills. I significantly benefited from their knowledge and inspiring motivation.

Dedication

To my family for always bringing out the best in me…

Abstract

The growth of cars purchasing power, typically gasoline cars, has been a serious contributor to greenhouse effect. Fuel usage reduction through transportation electrification is currently among the most vital research topics. Nevertheless, electric vehicle (EV) high prices and driving distance limitations, have been causing significant roadblocks to the EVs market evolution. Reducing the number of batteries in the EV would lead to lowering the EV's price, and decreasing the car's weight, which would increase the driving distance to charging time ratio. To make this feasible, EVs public chargers have to be widely available. This would enable users to charge their cars frequently, increasing the available driving distance. Wireless charging can be used to eliminate any risks of contact wearing or sparks during plugging/unplugging the wired charger. Wireless charging can be achieved through a transmitter embedded below the EV's parking slot, and a receiver fixed at the bottom of the EV. This thesis focuses on optimizing wireless charging through optimizing the coils geometry, and simulating the wireless power transfer process. Optimization was done using MATLAB optimization toolbox, and was double checked through mathematical derivation. A trend was obtained through the optimization process, which indicated that equal coils diameters results in maximum power transfer. The coils were designed on ANSYS Maxwell, with nine case scenarios having different geometrical values and change in radius, and their electromagnetic behavior was simulated. The full system, including the coils and the components of the electric circuit, was simulated at resonance frequency of 100 kHz, with the aid of ANSYS Simplorer. The amount of material used in the coils was calculated, as it affects the coils' prices. The coils weights were also calculated, as they affect the EV's consumed power. The introduced variable change in radius resulted in a 37% decrease in the coils weights to reach 26.5 kg, and a 37% decrease in the amount of material needed to manufacture the coils, to reach 2964 cm^3. The variable change in radius slightly increased the amount of power transferred by 0.75%, to reach 17.54 kW at perfect alignment between the coils, and 9 cm separation distance.

Keywords: ***Electric vehicle wireless charging; WPT optimization; electromagnetic simulation.***

Table of Contents

Abstract 6
List of Figures 11
List of Tables 14
List of Abbreviations 15
List of Symbols 16
Chapter 1. Introduction 17
1.1. Overview 17
1.2. Thesis Objectives 18
1.3. Research Contribution 19
1.4. Thesis Organization 19
Chapter 2. Background and Literature Review 20
2.1. Electric Vehicles' Market 20
2.2. Charging Systems Classification 20
2.3. Stationary Wired Charging 21
2.3.1. EVs batteries voltage levels and charging times. 21
2.3.2. Charging stations locations. 22
2.4. Dynamic Wired Charging 22
2.5. Stationary Wireless Charging 23
2.6. Dynamic Wireless Charging 25
2.7. Inductive Power Transfer vs. Capacitive Power Transfer 27
2.8. Wireless Power Transfer History 27
2.9. The Korean OLEV Project 28
2.10. Qualcomm Halo's Dynamic WPT Project 28
2.11. Coils Design 29
2.12. WPT Optimization 29
2.13. Resonance and Efficiency 30
2.14. Safety 31

Chapter 3. Methodology 33
3.1. Types of Coil Design 33
3.2. Mathematical Problem Formulation 34
3.3. Coil Weight Calculation Formula 37
3.4. Optimization Using MATLAB 40
3.4.1. Fmincon with interior point algorithm. 40
3.4.2. Fmincon with SQP algorithm. 40
3.4.3. Fmincon with active set algorithm. 40
3.4.4. Genetic algorithm. 41
3.5. Optimization Outcome Trends 43
3.6. Analytical Optimization 45
3.6.1. Analytical optimization procedure. 45
3.6.2. Power derivative zero crossing. 46
3.6.3. Double checking the zero crossing of the derivative function. 47
3.7. ANSYS Maxwell 50
3.7.1. ANSYS Maxwell features and capabilities. 50
3.7.2. ANSYS Maxwell simulation procedure. 51
3.8. Case Studies Designed on ANSYS Maxwell 52
3.8.1. Category A: constant change in radius in both coils. 52
3.8.2. Category B: variable change in radius in both coils. 52
3.8.3. Category C: variable change in radius in receiver coil only. 54
3.8.4. Case study - double receivers. 58
3.9. ANSYS Simplorer 58
3.9.1. ANSYS Simplorer features and capabilities. 58
3.9.2. ANSYS Simplorer simulation. 58
3.9.3. Resonance. 59
3.10. Relating Consumed Power to the Receiving Coil Weight 59

3.11. Relation Between Battery's State of Charge and its Internal Impedance.....60
3.11.1. Li-ion battery equivalent circuit model.....60
3.11.2. Parameters estimation.....61
3.11.3. Li-ion battery model simulation.....61
Chapter 4. Results.....65
4.1. ANSYS Maxwell Simulation Outcomes.....65
4.2. ANSYS Simplorer Simulation Outcomes.....70
4.2.1. Efficiency of no misalignment and constant change in radius.....70
4.2.2. Efficiency of 10% misalignment and constant change in radius.....70
4.2.3. Efficiency of 20% misalignment and constant change in radius.....70
4.2.4. Efficiency of no misalignment and variable change in radius in both coils.....72
4.2.5. Efficiency of 10% misalignment and variable change in radius in both coils.....72
4.2.6. Efficiency of 20% misalignment and variable change in radius in both coils.....72
4.2.7. Efficiency of no misalignment and variable change in radius in receiver coil.....74
4.2.8. Efficiency of 10% misalignment and variable change in radius in receiver coil.....74
4.2.9. Efficiency of 20% misalignment and variable change in radius in receiver coil.....74
4.3. Coils Weights and Material Volume.....74
4.3.1. Coil weight and volume in cases of a constant change in radius.....75
4.3.2. Coil weight and volume in cases of a variable change in radius.....75
4.4. Results Tabulation and Comparison.....75
4.5. Wireless Charging Time.....76

4.6. Comparison Between Different Coil Designs With Respect to the Consumed Power 76
4.7. Relation Between Battery's SOC and the Resonance Frequency 77
4.8. Current Delivered to the EV's Battery During Charging 78
Chapter 5. Conclusion and Future Work 79
5.1. Conclusion 79
5.2. Future Work 80
References 82
Vita 86

List of Figures

Figure 2.1: Suggested places for the usage of wireless charging [4]. 25
Figure 2.2: Wireless charging system [3]. 26
Figure 2.3: Wireless charging system cross section [3]. 26
Figure 2.4: Double transmitter WPT system [31].....30
Figure 2.5: Multi-receivers WPT system [32].....30
Figure 2.6: WPT three main stages [33]. 31
Figure 3.1: Different types of coil design [34]. 33
Figure 3.2: Electric lines of force cutting the conductor normally [34]. 34
Figure 3.3: Coils dimensions annotation. 35
Figure 3.4: WPT equivalent circuit for maximum power transfer. 35
Figure 3.5: WPT equivalent circuit with source transformation done on the secondary side.....35
Figure 3.6: Delivered power vs. distance between transmitting and receiving coils...37
Figure 3.7: Delivered power vs. displacement between the centers of transmitting and receiving coils.....37
Figure 3.8: Angle of rotation. 38
Figure 3.9: Coil's starting radius.....38
Figure 3.10: Coil's change in radius.....39
Figure 3.11: MATLAB optimization outcomes with fmincon interior point. 41
Figure 3.12: MATLAB optimization outcomes with fmincon SQP. 42
Figure 3.13: MATLAB optimization outcomes with fmincon active set. 42
Figure 3.14: MATLAB optimization outcomes with Genetic Algorithm. 43
Figure 3.15: Power derivative vs. receiver diameter at transmitter diameter of 0.8 meter. 47
Figure 3.16: Power derivative vs. receiver diameter at transmitter diameter of 1 meter. 48
Figure 3.17: Power derivative vs. receiver diameter at transmitter diameter of 1.2 meter. 48
Figure 3.18: ANSYS Maxwell automatic meshing 50
Figure 3.19: Transmitting and receiving coils in ANSYS Maxwell 53
Figure 3.20: Side view of the coils on Maxwell.....53

Figure 3.21: Top view of the coils on Maxwell. 54
Figure 3.22: Top view of the coils on Maxwell. 54
Figure 3.23: Top view of the coils on Maxwell. 54
Figure 3.24: Transmitting and receiving coils with a variable change in radius. 55
Figure 3.25: Top view with a variable change in radius. 55
Figure 3.26: Variable change in radius in both coils and a 10% misalignment. 55
Figure 3.27: Top view with variable change in radius in both coils and a 10% misalignment. 55
Figure 3.28: Top view of the coils on Maxwell. 55
Figure 3.29: Receiving coil of a variable change in radius and transmitting coil of a constant change in radius. 56
Figure 3.30: Top view of the receiving coil of a variable change in radius and transmitting coil of a constant change in radius. 56
Figure 3.31: Transmitting and receiving coils with a variable change in radius and a 10% misalignment. 56
Figure 3.32: Top view with a variable change in radius and a 10% misalignment. 56
Figure 3.33: Transmitting and receiving coils with a variable change in radius and a 20% misalignment. 57
Figure 3.34: Top view with a variable change in radius and a 20% misalignment. 57
Figure 3.35: Double receiving coils designed using ANSYS Maxwell. 57
Figure 3.36: Top view of double receiving coils designed using ANSYS Maxwell. ..57
Figure 3.37: Full circuit implementation on ANSYS Simplorer. 59
Figure 3.38: Equivalent circuit model for Li-ion battery [42]. 61
Figure 3.39: Simulink Li-ion battery model [43] 62
Figure 3.40: Battery's SOC vs. Time. 62
Figure 3.41: Battery's voltage vs. Time.....64
Figure 3.42: Battery's voltage vs. Battery's SOC. 64
Figure 4.1: Simulation of WPT taking place between the transmitter coil embedded underground, and the receiver coil fixed at the bottom of the car. 65
Figure 4.2: Field plot for case study 1 using ANSYS Maxwell simulation. 66
Figure 4.3: Field plot for case study 2. 67
Figure 4.4: Field plot for case study 3. 67
Figure 4.5: Field plot for case study 4. 67

Figure 4.6: Field plot for case study 5. 68
Figure 4.7: Field plot for case study 6. 68
Figure 4.8: Field plot for case study 7. 68
Figure 4.9: Field plot for case study 8. 69
Figure 4.10: Field plot for case study 9. 69
Figure 4.11: ANSYS Simplorer outcomes for case study 1. 71
Figure 4.12: ANSYS Simplorer outcomes for case study 2. 71
Figure 4.13: ANSYS Simplorer outcomes for case study 3. 71
Figure 4.14: ANSYS Simplorer outcomes for case study 4. 72
Figure 4.15: ANSYS Simplorer outcomes for case study 5. 72
Figure 4.16: ANSYS Simplorer outcomes for case study 6. 73
Figure 4.17: ANSYS Simplorer outcomes for case study 7. 73
Figure 4.18: ANSYS Simplorer outcomes for case study 8. 73
Figure 4.19: ANSYS Simplorer outcomes for case study 9. 74
Figure 4.20: Power transferred with battery SOC varying from 1 to 0.2. 77
Figure 4.21: Power transferred with a battery SOC of 0.1. 78
Figure 4.22: Maximum current delivered to the battery during charging. 78

List of Tables

Table 2.1: Voltage levels and charging times of different EVs models using wired charging [8]. 22
Table 2.2: Cost comparison between plug-in and wireless charging stations [4]. 25
Table 3.1: Optimization of the transmitting coil diameter. 44
Table 3.2: Optimization of the transmitting and receiving coils diameters. 44
Table 3.3: Optimization of the transmitting coil diameter and the wire radius.....44
Table 3.4: ANSYS Maxwell simulation parameters.....53
Table 3.5: ANSYS Maxwell simulation parameters.....53
Table 3.6: ANSYS Maxwell simulation parameters.....56
Table 3.7: Parameters for a 400 V Li-ion battery bank [42]. 63
Table 3.8: Battery's voltage and equivalent impedance at different values of SOC...63
Table 4.1: ANSYS Maxwell results. 66
Table 4.2: ANSYS results. 76

List of Abbreviations

CHR	Change in Radius
CPT	Capacitive Power Transfer
ESS	Energy Storage System
EV	Electric Vehicle
IPT	Inductive Power Transfer
OLEV	Online Electric Vehicle
SOC	State Of Charge
WPT	Wireless Power Transfer

List of Symbols

a	Coil’s wire radius
c	Starting Radius of Coil
d_1	Transmitter Coil Diameter
d_2	Receiving Coil Diameter
h	Separating Distance Between Transmitter and Receiver
I_1	Current in Primary Circuit
l	Total Length of Coil’s Wire
R_L	Load Resistance
x	Misalignment Between the Centers of Transmitter and Receiver

Chapter 1. Introduction

In this chapter, an introduction to electric vehicles, and their charging systems, is provided. Following this, the problem at hand is addressed as well as the research objectives, aims, and contributions. Finally, the organization of the thesis is presented.

1.1. Overview

Over the past few years, sustainability became a vital consideration all over the world. The world is facing the risk of running out of nonrenewable energy. This led to the necessity of finding alternatives. Moreover, pollution and climate change impacts push for environmentally friendly solutions. In February 2015, China's ministry of science and technology targeted having 5 million electric vehicles on China's roads by the year 2020. Unfortunately, as we approach the end of 2019, the number of EVs in China is around 1.6 million [1]. This shows how shifting away from gasoline as an energy source for cars, is a tough challenge. This is mainly due to the gasoline's high energy density, which is around 120 times the energy density of lithium-ion batteries. That is why some improvements should be done to decrease EVs limitations.

A main field of improvement is the charging systems. One already applied solution is electric plug-ins for EVs in malls' and universities' parking areas. This permits the usage of parking time for charging the batteries. However, different electrical cars require different plug receptacles, which sometimes causes inconvenience, and limits the benefits of that solution. This is why the wireless power transfer (WPT) technique became a center of interest. The main challenge of this technology is to transfer energy from the source (transmitter) to the load (receiver) through an air gap.

The advantages of wireless charging are many, such as eliminating the problem of incompatible plug receptacles, reducing any sparks risk, and avoiding any contact wearing. WPT is classified into stationary charging EVs (SCEVs), and dynamic charging EVs, referred to as roadway powered EVs (RPEVs). For the stationary charging system, the driver parks their car over the designed area, and leaves, while their car gets charged. Stationary wireless charging can also be used to charge an electric bus while passengers embark and disembark. While for the dynamic charging system, the car is charged while being driven [2]. Dynamic wireless charging has the

advantage of reducing the stoppage time needed for charging, and increasing the reliability by increasing the possible driving distance.

The heavy bulky energy storage system (ESS) has been a main roadblock to the efficiency of EVs. A competitive solution for this issue is to have widely available public chargers, to enable users to charge their car batteries more frequently, and therefore increase the available driving distance. Another solution is to have electrified roads, delivering power continuously to EVs while they're being driven. This can be done wirelessly through transmitters embedded below the road surface and receivers fixed at the bottom of the EVs [3]. Because indeed, if the recharging is done frequently or even online, then there's no need for bulky batteries. Bulky batteries will only be needed when driving on a road where there are no public chargers, or in an area where the dynamic WPT system is not available [4]. The reduction of the number of batteries would lead to decreasing the weight, which would increase the efficiency and increase the ratio of driving to charging time. Decreasing the number of batteries would also clearly lower the EVs prices, therefore attract more consumers, making it possible for electric cars manufacturers to further lower the prices through mass production.

One more area for improvement lies in the incentives provided by governments to encourage people to use EVs. Norwegian government, as an example, offers extremely smart and generous incentives to EVs owners. This includes toll-free roads, high occupancy vehicle lane access without being highly occupied, free parking, and free charging [6]. As a result of these incentives, Norway has climbed up to the top of the market share, where 49.1% of cars on the Norwegian roads are electric [7].

1.2. Thesis Objectives

In this research, the equation which describes the power delivered to the car's battery through WPT, in terms of the coils geometry, is derived. This equation is used to construct the objective function which serves the optimization problem. Different constraints are applied to ensure the geometrical feasibility of the design, for instance, the diameters of the transmitter and receiver coils and the radius of the conductor used. This would ensure the feasibility of placing the receiver coil at the bottom of the EV, in addition to minimizing its weight, and on the other hand minimizing the price of manufacturing the coils. The optimized geometrical parameters are used to design the coils on ANSYS Maxwell, and simulate the electromagnetic behavior between the

transmitter and receiver coils in 3D. This is done using finite element method, which results in calculating the coupling coefficient between the coils, as well as the coils' self-inductances, which are necessary to design a resonating circuit later on. A novel idea is introduced, where coils having a variable change in radius between their turns are designed and simulated. Furthermore, ANSYS Simplorer is used to simulate the full transmitter-receiver circuit to obtain the power received by the car battery.

The main benefits behind these outcomes is that they can be used by the EV manufacturers to design their coils. In addition, electricity utility companies can use the obtained results from this research, to set billing scenarios for customers willing to charge their cars wirelessly.

1.3. Research Contribution

The contributions of this research can be summarized as follows:

- Providing optimized coil designs for stationery WPT
- Introducing a variable change in radius between the coils turns
- Evaluating different types of coil designs, and comparing their power transfer efficiency
- Testing the charging circuit at resonance frequency

1.4. Thesis Organization

The rest of the thesis is organized as follows: chapter 2 provides literature review and background information about existing EV wireless charging, and the current research venues in this field. The proposed methodology and optimization algorithms are presented in chapter 3. The outcomes and results are presented in chapter 4. Finally, chapter 5 discusses the thesis conclusion and presents the outlines for the future work.

Chapter 2. Background and Literature Review

This chapter is going to cover the current status of wireless charging of EVs. It will provide information about the previous studies concerned with static and dynamic wireless power transfer. In addition, the current state-of-the-art in WPT, will be pointed out and clearly reported. The following flowchart briefs the chapter's outlines.

2.1. Electric Vehicles' Market

Similar to any commercial market, the EVs market's aim is to maximize the profit resulting from EVs selling. In reality, EVs market is not reaching that aim. This is mainly due to the high prices of EVs. The main contributor to that high price is the battery, which is difficult to design as it has to have high energy and power densities, long life time, high safety, and high reliability. The compromise between the driving range of the EVs and their batteries size is considered a loop; whereas for the EV to be able to drive long distances, a large number of batteries is needed. This translates into higher price of the EV. Moreover, a larger number of batteries translates into a heavier weight of the EV, which leads the EV to consume more power, resulting in faster discharging of the batteries, and thus shorter driving range.

This is why the wireless power transfer (WPT) technique became a center of interest. The wireless power transfer, also known as wireless charging, has been a hot topic and gained much attention from governments, and research groups around the world. The main challenge of this technology is to transfer energy from the source (transmitter) to the load (receiver) through an air gap. Electric vehicles are most popular in the United States, where it has been the largest and most active EV market in the world for the past few years. This is driven by the government's goals of decreasing air pollution. Moreover, automotive industry is aiming at providing more environmentally friendly and energy-efficient EVs [8].

2.2. Charging Systems Classification

Charging systems are classified into wired charging and wireless charging. Wired charging systems can be classified intro stationary wired charging and dynamic wired charging. On the other hand, wireless charging is based on WPT, which is classified into dynamic charging EVs, referred to as roadway powered electric vehicles

(RPEVs), and stationary charging electric vehicles (SCEVs). For the stationary charging system, the driver parks the car over the designated area, and leaves. While for the dynamic charging system, the car is charged while being driven, which theoretically can mean running forever without stopping [9]. WPT is also classified into inductive power transfer (IPT) and capacitive power transfer (CPT).

2.3. Stationary Wired Charging

Unlike gasoline and diesel cars, EVs are powered exclusively by rechargeable batteries. One method of charging is using electricity charging stations. These static stations are classified into three different power levels: level 1, level 2, and DC fast charging, depending on how quick they are capable of charging. Level 1 is the basic charging station, which provides 110 V at a maximum power of 3.3 kW. Level 2 raises the charging voltage to 240 V at a maximum power of 19.2 kW. DC fast charging stations provides 480 V at a maximum power of 50 kW. DC fast charging stations have the ability to charge most EVs from zero to 80% in under 30 minutes [8].

2.3.1. EVs batteries voltage levels and charging times. This section will briefly put across the different voltage levels of electric vehicles' batteries, and their charging times. The vast majority of electric vehicles use the 300 V - 400 V range. Very few electric vehicles use the 750 V - 800 V range. Reasonable diameters of cable at high amperage can be achieve by raising the voltage. However, anything above 600 V starts to get exotic in terms of insulation, where components and materials become significantly more expensive due to the high ratings. Table 2.1 shows the voltage levels and charging times of different electric vehicles models, using wired chargers.

As shown, the voltage of EVs batteries ranges from 200 V to 400 V. As an example, in the Chevy volt, the controller takes in 30 V DC from the battery pack and converts it into three-phase 240 V AC, then sends it to the motor. Very large transistors are used in the inverter to create a sine wave from the DC voltage. The manufacturers of Nissan Leaf, BMW i3 and other EVs use lithium-manganese (LMO) battery with an NMC blend. Tesla uses NCA (nickel, cobalt, aluminum), and to protect the delicate Li-ion from over-loading at highway speed, the battery pack is over-sized by around three fold compared to other EVs. The large 90 kWh battery of the Tesla

Table 2.1: Voltage levels and charging times of different EVs models using wired charging [8].

EV model	Battery ratings	Charging times
Toyota Prius	4.4 kWh Li-ion 201.6V	3h at 115 VAC 15 A 1.5h at 230 VAC 15 A
Chevy Volt	16 kWh Li-manganese NMC 300 V, 181kg	10h at 115 VAC, 15 A 4h at 230 VAC, 15 A
Mitsubishi iMiEV	16 kWh Li-ion 330 V	13h at 115 VAC 15 A 7h at 230 VAC 15 A
BMW i3	22 kWh LMO/NMC 360 V, 204kg	4h at 230 VAC 30 A 30 min for 80% at 50 kW Supercharger
Nissan Leaf	30 kWh Li-manganese 380 V, 272kg	8h at 230 VAC, 15 A 4h at 230 VAC, 30 A
Tesla S	90 kWh NCA (nickel, cobalt, aluminum) 400 V, 540kg	9h with 10 kW charger 30 min for 80% at 120 kW Supercharger

S Model (2015) provides a driving range of 424 km, nevertheless, the battery weighs 540 kg, resulting in the highest energy consumption among EVs at 238 Wh/km. In comparison, 160 Wh/km is the energy consumption of the BMW i3, one of the lightest EVs. It uses an LMO/NMC battery that provides a driving range of 130 to 160 km. In addition, 750 V to 800 V range was tried out. However, it was too exotic and expensive in terms of insulation.

2.3.2. Charging stations locations. Installing more EV charging stations could have a direct effect on boosting the sustainability of our world, through attracting more people to use EVs [8]. Several practical issues will have to be planned for during the design of charging station and before the installation phase. One important issue is where to install the charging stations.

2.4. Dynamic Wired Charging

Sweden's 2050 goal is to be carbon neutral. For this goal's progress, the Swedish authorities have modified approximately 2 km of road to charge EVs on the go, to become the world's first electrified road. Road transport accounts for more than 30% of Sweden's carbon emissions [10]. Unfortunately, things are not that easy. Vehicles have to be equipped with a special arm that contacts a rail stretched on the

road to get the electricity. The system is similar to the third rail used by electric trains to get its electricity, or the overhead wires for trams, with the difference in the location of the wires of rails. The charge is transferred from two tracks of rail on the road through a movable arm attached to the bottom of the EV. Should the vehicle overtake or change lanes, the arm is automatically disconnected. The rails are divided into 50m sections, so that the section is only powered when a vehicle is charging from it. As for the safety, the electricity path is kept way of the surface where a barefoot can walk. This is because the path which acts as an outlet for electricity is found five to six centimeters down between two surface tracks. Even if you flood the road with salty water, the surface voltage will always stay below one volt, which is safe enough not to cause any damages, injuries, or electric shocks [11].

Sweden has around 500,000 km of roads, including only 20,000 km of highways. The project was to only equip the highway portions of roads with the rail charging system. Yet, the high cost of €1m per kilometer led to stopping the project after trying 2 km only. This wasn't the first time Sweden contributed in charging systems for moving EVs. Previously, Siemens installed overhead wires over a portion of a road, where trucks were equipped with pantographs, similar to the ones in electric trains and trams, which contacted the wires and transmitted the electricity. Both projects use trucks as test vehicles, which shows Sweden’s interest in using electric trucks.

2.5. Stationary Wireless Charging

The benefits of stationary wireless charging are many, such as eliminating the problem of incompatible plug receptacles, reducing any sparks risk, and avoiding any contact wearing. Stationary wireless charging can also be used to charge an electric bus while passengers embark and disembark, as shown in Figure 2.1. This can also be implemented in sections of the roads in high-congested areas, or at traffic lights, or drive-through lanes, where the vehicle speed is low [4].

At the University of Hong Kong, Dr. Ron Hui together with his team performed research on planar low power inductive battery chargers [12]-[13]. At the same time in Auckland New Zealand, Dr. Covic and Dr. Boys started examining high power WPT applications for mostly static charging. They succeeded in publishing numerous patents

and journal papers, which describe and highlight multiple aspects of the WPT technology. They looking into power electronics, various circuit topologies, and coil designs [14]-[15][16][17][18].

EVATRAN company has developed Plugless inductive charging system for stationary rapid charging and is commercializing it in the partnership with Bosch. It consists of a power transmitting pad placed under the vehicle and a control panel linked to a 240 V, 30 A electrical power supply. The system guides the driver to park over the charging pad, and in addition displays the battery state of charge. The Department of Energy (DOE) in Idaho Engineering Lab tested the system's technical specifications and safe operability. They confirmed that it complies with the safety limits of EMF human exposure. Up to date, testing has been done for more than 1,500 hours of plugless power charging using electric Chevy VOLT and Nissan Leaf cars.

There are five factors to be reviewed and examined when developing commercial wireless chargers across a city, instead of plug-in chargers. Firstly, a wireless charging station costs approximately $1,300 more than a plug-in charger level 1, excluding the station installation fee, as they require 208/240 V input voltage and a 30 A breaker. The station installation fee depends on several factors such as the electrician labor and the materials cost. Table 2.2 shows the installation cost comparison for plug-in and wireless chargers [4].

The second factor is regarding the regulations where some EV manufacturers have not yet equipped their EVs with WPT receiving coils. Some commercial WPT coils are installed through a third party, but this may violate the car warranty and therefore stop customers from using this alternative solution. Technology Adoption and improvements is the third factor to be considered. Customer feedback on the wireless charging experience was collected and analyzed; most drivers found difficulty in aligning the car with the charging pads, so they had to readjust their parking multiple times, which consumed time and resulted in an unpleasant experience. Pricing policy is the fourth factor that EVs owners consider when using public charging. Some pricing policies can encourage efficient use of public EV chargers to minimize idle time. Optimization of charging station locations according to users' distribution is the fifth factor, as it could help extend the EVs' driving range. The optimal locations of wireless

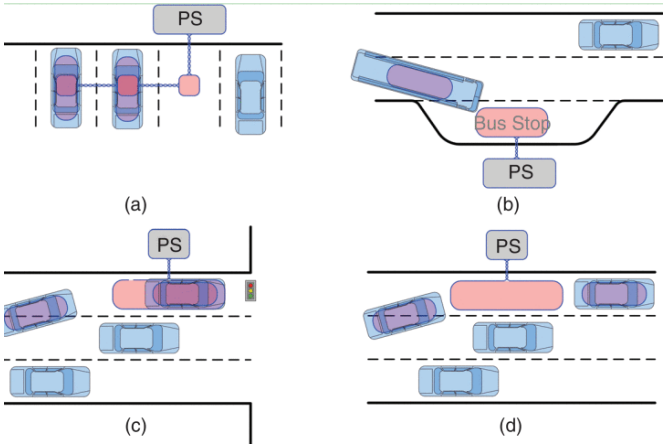

Figure 2.1: Suggested places for the usage of wireless charging [4].

Table 2.2: Cost comparison between plug-in and wireless charging stations [4].

Items	Plug-in	Wireless
Charger	~$900	$1940
Car installation fee	N/A	$300
Station installation fee	N/A	$2000

charging stations should be places with the largest traffic density, largest parking demands, or places where visitors and travelers mostly stay, like student centers, business centers, malls, hotels, drive-through lanes, and sports stadiums.

Currently, BMW 530e iPerformance model can be fully reloaded in three and a half hours, at 11 kW of stationary wireless charging. Tesla S model can be charged with 7.2 kW per each hour of stationary wireless charging [19]-[20]. Research is going on in Oak ridge National Laboratory to reach a 120 kW EV static wireless charger. This is equivalent to a Tesla wired supercharger.

2.6. Dynamic Wireless Charging

Dynamic wireless charging has numerous benefits, such as reducing the stoppage time needed for charging, increasing the reliability through increasing the possible driving distance, and most important, making it possible to reduce the number of batteries. The heavy bulky energy storage system (ESS) has been a main roadblock to the efficiency of EVs. A competitive solution for this issue is to have electrified roads, delivering power continuously to EVs while they're being driven. This can be

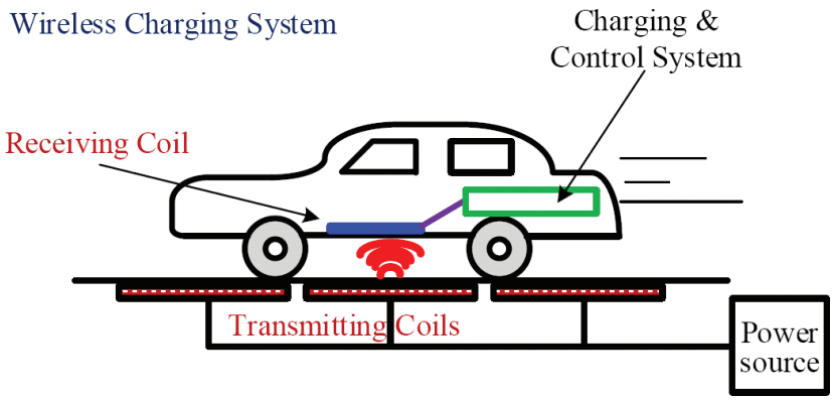

Figure 2.2: Wireless charging system [3].

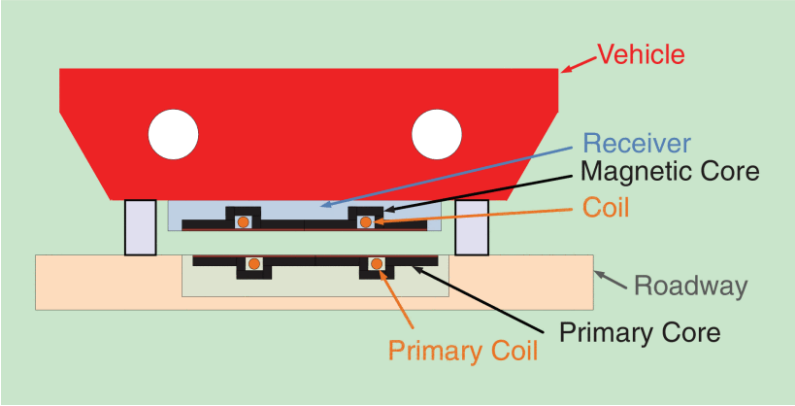

Figure 2.3: Wireless charging system cross section [3].

done wirelessly through transmitters embedded below the road surface and receivers fixed at the bottom of the EVs as shown in Figures 2.2 and 2.3 [3].

Indeed, if the recharging is done online, then there's no need for bulky batteries to support the whole driving range. Batteries will only be needed to supply power when driving in an area where the WPT system is not available [4]. The reduction of the number of batteries would lead to decreasing the weight, which would increase the efficiency and increase the ratio of driving to charging time. Decreasing the number of batteries would also clearly lower the EVs prices, therefore attract more consumers, making it possible for electric cars manufacturers to further lower the prices through mass production.

2.7. Inductive Power Transfer vs. Capacitive Power Transfer

As mentioned before, WPT can be classified into two major categories which are inductive power transfer (IPT) and capacitive power transfer (CPT). Magnetic induction based IPT tends to have poor efficiency when the coils are misaligned. CPT technologies tend to require high switching frequencies (>1 MHz) that can limit the practically realizable power levels [21]-[22][23]. For EV charging applications, magnetic resonance based IPT is currently the preferred technology [24]-[25][26].

2.8. Wireless Power Transfer History

Going back in history, exactly 1891, Nikola Tesla invented the famous Tesla coil. Briefly, Tesla invented a system of two tuned resonant circuits, a large, single layer primary and secondary (which reduces the resistance significantly), loosely coupled. To further understand the difference between loosely coupled and tightly coupled coils, the coupling medium needs to be mentioned. When the coupling medium is air, the coupling coefficient drops to 0.1 to 0.2 (depending if it is stationary or dynamic WPT), this is referred to as loosely coupled. Contrarily, when the coupling medium is a ferromagnetic material, such as in transformers, the primary and secondary coils are said to be tightly coupled.

Three years later after Tesla's work, Hutin and LeBlanc showed how a transformer can be used to power streetcars with no contact, using an elongated single-wire coil acting as a primary carrying 2 kHz AC with multiple secondary windings. They used suspension systems to decrease the distance between the primary and secondary sides, plus ferromagnetic materials to increase the coupling. This system didn't not succeed commercially due to component limitations at that time. Moving to the 1990s, researchers from University of California built a 120 meters powered proof-of-concept roadway, with a primary side powered with 1200 Amps, 400 Hz AC current, and a receiver (pickup) at a distance of 7.6 cm. In 1992, they worked on Advanced Transit and Highways (PATH) program. A deep investigation and practical tests were performed on RPEVs and the PATH team came up with the first RPEV buses. The maximum efficiency reached was 60% but the low frequency limited the size of the system. A few years later, in Auckland New Zealand, Dr. Covic and Dr. Boys published several patents and papers concerned with high power WPT applications, they focused

on static power transfer. These papers talked about the power electronics used, different circuit topologies, and coil designs.

2.9. The Korean OLEV Project

Different researched and trials were done until 2008, when Korean researchers in the Advanced Institute of Science and Technology (KAIST) used different ferromagnetic materials and a different track layout to reach a peak efficiency of 70%. Then they developed an online electric vehicle (OLEV), with an output power of 60 kW with a large air-gap of 20 cm (7.6 cm previously in the PATH project). Moreover, the construction cost of the power rail for the OLEV, which accounts for 80% of the total cost for RPEVs, dramatically fell down to around one third of that of the PATH project. The first OLEV commercial version was announced in 2009 when it was used in a trolley system in Seoul city. The second version was introduced in 2012 for shuttle buses on the KAIST campus. Moving to 2013, specifically in Gumi City, two OLEV buses were developed and used on a metro bus line. Last but not least, an OLEV bus started working in Sejong in 2015 [27].

Therefore to sum up, the South Korean OLEV is one of the best approaches done, where the efficiency is so high that it will enable buses to use batteries which are about one third the size of what is found in electric cars. That's far smaller and lighter than what a conventionally charged electric bus would require [27].

2.10. Qualcomm Halo's Dynamic WPT Project

One should wonder, how would this be used in a Tesla for example, which is not equipped with a movable charging arm. To make matters worse, having a movable charging arm would be much more expensive than dynamic wireless charging. This is why Qualcomm Halo company took advantage of the Formula E race which took place in Paris to show off their dynamic wireless charging project they've been working on for the past few years [30]. Mercedes is expected to be the first that uses the technology developed by Qualcomm Halo. Qualcomm is testing a solution using 2 receiving coils for robustness, but in reality, one receiving coil is enough. Qualcomm was able to prove by experiment that dynamically charging multiple moving EVs having uneven alignments on the same road is possible.

2.11. Coils Design

The significant breakthrough in the development of wireless charging was made by a large number of research groups, however, its efficiency was still not satisfactory. The shapes of coils and ferrites are the keys to study the coupling, which is the main influencer on the power efficiency. The design impacts the power capacity transferred between the two sides of the coupler. The magnetic structures are used to enhance coupling, reduce flux leakage and shape the magnetic field.

Researchers from China studied the differences between using planar square coils, planar circular coils, and solid spiral coils. They found that sharp edges causes non-uniform magnetic and electric fields. As known, any conductor is equipotential, so electric lines of force always cut the conductor normally. Consequently, at sharp edges, the lines of force get closer to each other, to keep cutting the conductor normally. This explains the non-uniformity caused by sharp edges. And since E = V/d, where d is distance between equipotential lines, therefore the smaller the radius of curvature, the greater the concentration of charges, the stronger the electric field [30]. As for the solid spiral coils, magnetic flux density is maximum at the spiral's core, while it is weak at the top of the three-dimensional spiral structure, as the distribution area is wide. This leads to a reduced power transfer for applications where the coupling happens at the top of the spiral coil, and that's the case for EV wireless charging. Finally, it was found that planar circular coils have the highest magnetic flux density with a uniform magnetic field.

2.12. WPT Optimization

System optimization for WPT was carried out by different researchers with different point of views and with taking different aspects into consideration. A group of researchers in China proposed a WPT system with double transmitters [31]. They implemented an experimenting set up, shown in Figure 2.4, with 10 cm spacing between each transmitter and the receiver. They reached an efficiency of 91%. Nevertheless, this topology is not applicable for the application of EV wireless charging, where it is not feasible to have the receiver placed between 2 transmitters.

Another group of researchers, again in China, proposed a WPT system with multi-receivers. In other words, an array of 3 receiving coils, as shown in Figure 2.5.

This topology achieved 89.5% efficiency, but that was done at only 2 cm spacing between the transmitter and the array of receivers [32].

2.13. Resonance and Efficiency

Using magnetic resonant coupling between the primary coil placed in the ground and the secondary coil placed in the car for WPT can be fast and above 80% efficient. The three main stages of WPT is illustrated in Figure 2.6.

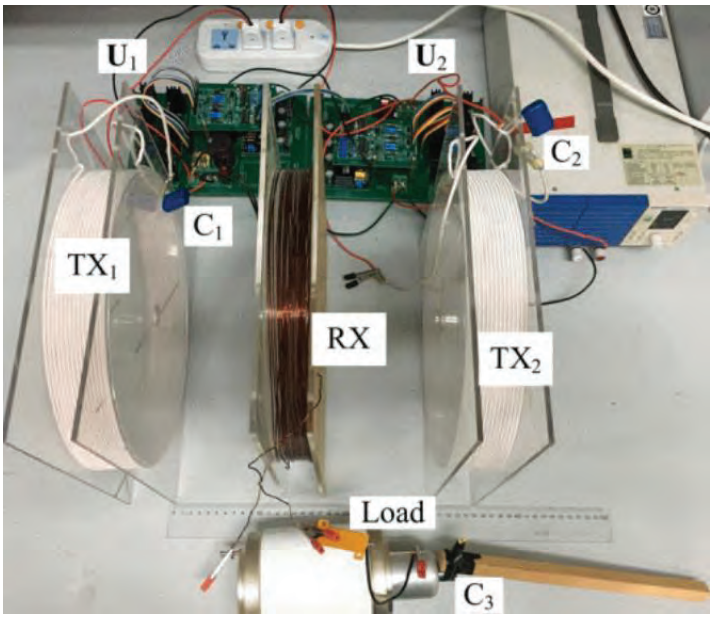

Figure 2.4: Double transmitter WPT system [31].

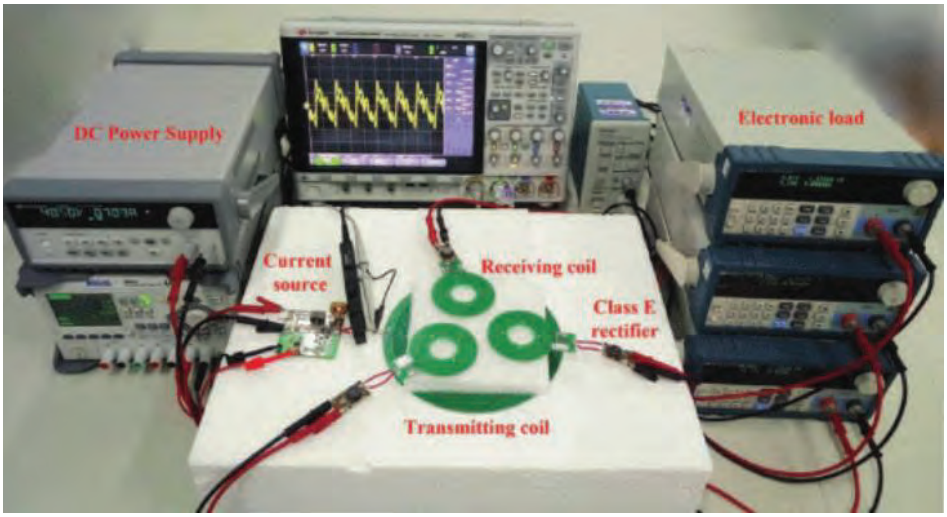

Figure 2.5: Multi-receivers WPT system [32].

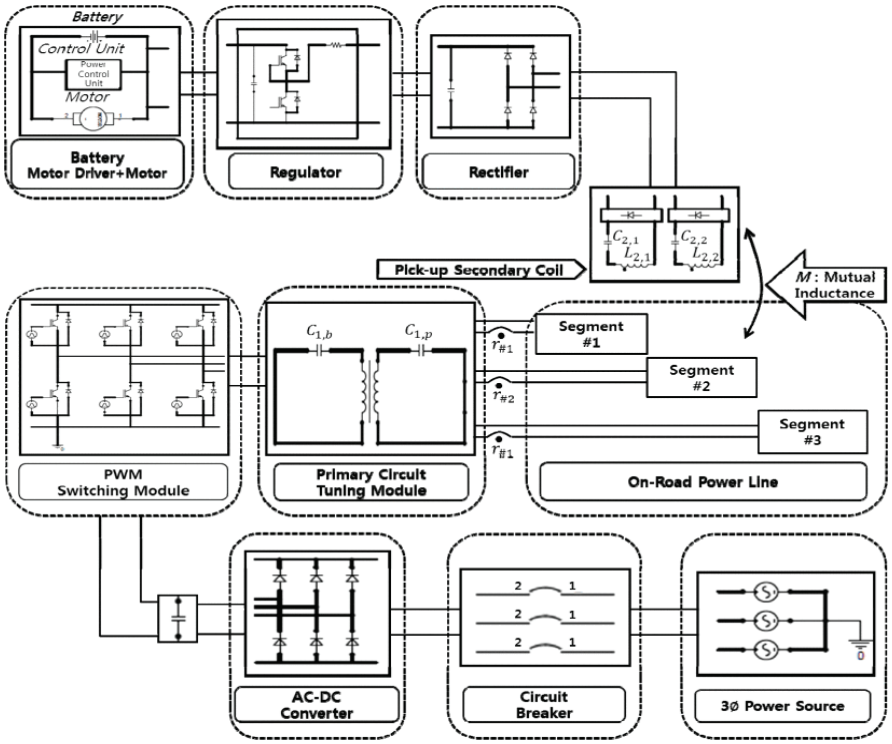

Figure 2.6: WPT three main stages [33].

Firstly, AC is converted to DC using an AC to DC converter, then a compensating circuit is used to get high frequency AC power from the DC power. Secondly, the high frequency AC in the primary side generates an alternating magnetic field which induces an AC voltage on the secondary side, used to charge the battery. Resonance in employed to boost up the WPT. By resonating plus using a DC/DC converter on the secondary side, efficiency of WPT is improved significantly. In addition, Leakage inductance between the primary and secondary coils results in poor efficiency of power transfer. This leakage inductance can be minimized by applying reactive current compensation between the primary and secondary coils. This is done using compensation capacitors.

2.14. Safety

Safety indeed needs to be well considered in WPT, as the coils will be part of the roads or parking areas, and therefore they need to follow some regulations. For example, the material covering the surface of the road or parking area should resist water. Moreover, the coils should be able to support the weights above it, and they

should be waterproof in case any water leakage occurred. Furthermore, the coils should be reliable to avoid maintenance, yet they shouldn’t interfere with the road maintenance.

Chapter 3. Methodology

This chapter will cover the steps and procedures that will be followed to achieve the target of this research. It starts with clarifying the different types of coil design, and which one is chosen for this research. Next, the problem formulation is mathematically approached. Afterwards, both analytical optimization and optimization using MATLAB are discussed. The usage of ANSYS Maxwell is then elaborated together with the case studies conducted in this research. ANSYS Simplorer usage is also discussed in conjunction with the electric circuit used for simulation and how resonance is achieved. The relation between the coil weight and EV power consumption is also addressed. Finally, Li-ion battery model and the relation between the battery's SOC and internal impedance are discussed. The following flowchart summarizes the chapter's topics.

3.1. Types of Coil Design

Three main types of coil design were looked into: the planar square coil, the planar circular coil, and solid spiral coil, as shown in Figure 3.1. The issues that come with the planar square coil are several. One of the most significant is its non-uniform magnetic and electric fields, which is caused by sharp edges. The conductor has to be equipotential, so electric lines of force always cut the conductor normally, as shown in Figure 3.2. At sharp edges, the lines of force are closer to each other to keep cutting the conductor normally [34]. The smaller the radius of curvature, the greater the concentration of charges and the stronger the electric field $E = V/d$, where d is distance between equipotential lines.

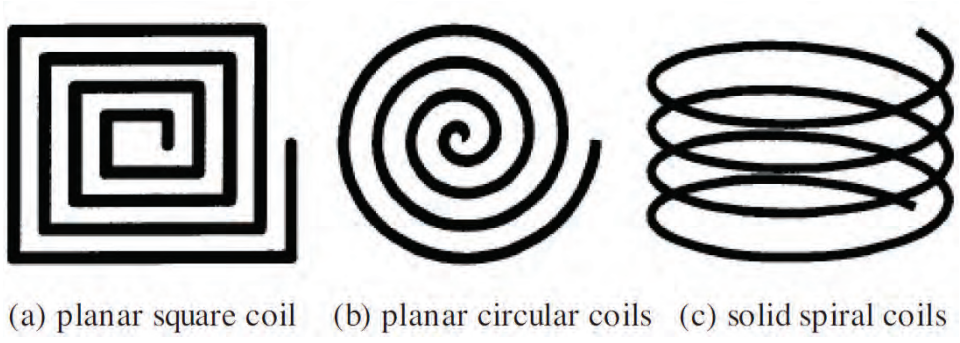

Figure 3.1: Different types of coil design [34].

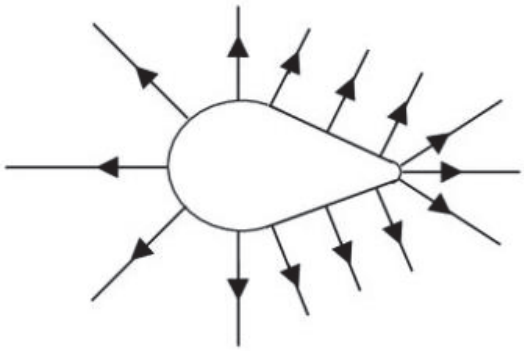

Figure 3.2: Electric lines of force cutting the conductor normally [34].

Magnetic flux density at the top of the three-dimensional spiral structure is weak, as the distribution area is wide, which makes it inefficient for EVs wireless charging. Planar circular coil is the most convenient for EVs wireless charging, where it provides the highest magnetic flux density with a uniform magnetic field. This is why this research will focus on planar circular coils.

3.2. Mathematical Problem Formulation

Mutual inductance equation used for this research was proven through calculations and experiments [35]. It states that:

$$M = \frac{\mu_o}{2\pi} \ ln \frac{r_2 r_3}{r_1 r_4} \tag{3. 1}$$

$$r_1 = \sqrt{h^2 + x^2} \tag{3. 2}$$

$$r_2 = \sqrt{h^2 + (x + d_2)^2} \tag{3. 3}$$

$$r_3 = \sqrt{h^2 + (d_1 - x)^2} \tag{3. 4}$$

$$r_4 = \sqrt{h^2 + (x + d_2 - d_1)^2} \tag{3. 5}$$

Where M is the mutual inductance, h is the separation distance between coils, x is the displacement, d_1 & d_2 are the diameters of the coils, as shown in Figure 3.3.

The aim here is to get the power delivered to the EV batteries through wireless charging, as this is what is targeted to be maximized. For that, the load voltage, which is the voltage reaching the secondary side of the circuit, needs to be formulated. The circuit in Figure 3.4 was used as it results in maximum power transferred to the load.

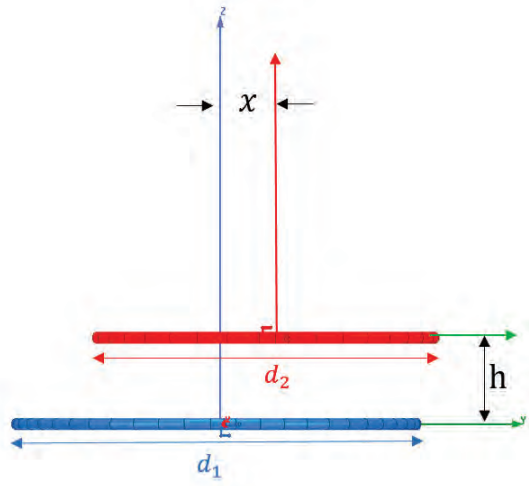

Figure 3.3: Coils dimensions annotation.

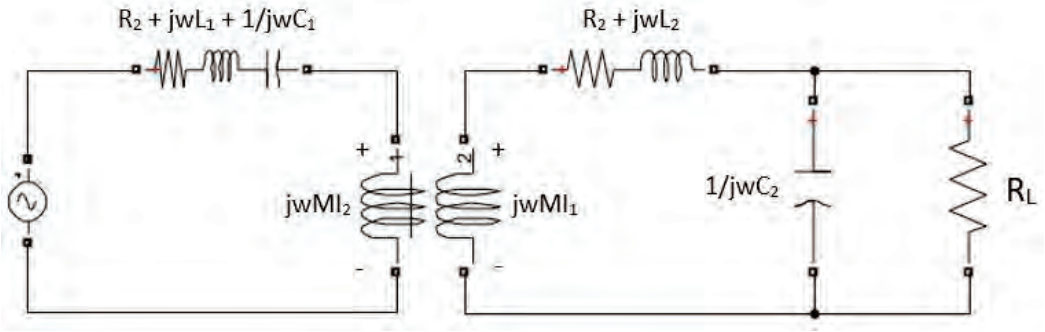

Figure 3.4: WPT equivalent circuit for maximum power transfer.

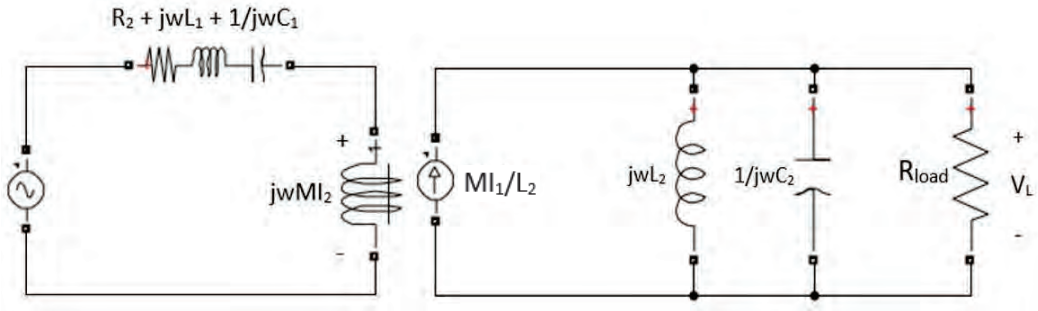

Figure 3.5: WPT equivalent circuit with source transformation done on the secondary side.

Source transformation was done on the secondary side of the circuit, as shown in Figure 3.5. Load voltage V_L can thus be formulated as:

$$V_L = \frac{M}{L_2} I_1 Z = \frac{M I_1}{Y L_2} \quad (3.6)$$

Where $Z = \frac{1}{Y}$ is the impedance seen by the current source, and where admittance Y is in this case formulated as:

$$Y = \frac{1}{j\omega L_2} + j\omega C_2 + \frac{1}{R_L} \quad (3.7)$$

As for the inductance:

$$L_2 = \frac{\mu_o}{\pi} \left[0.25 + ln \frac{d_1}{a}\right] \quad (3.8)$$

Where d_1 is the diameter of the primary coil, and a is the radius of the coil wire. Finally, since the voltage reaching the EV battery is:

$$V_L = \frac{M I_1}{L_2} R_L \quad (3.9)$$

Therefore, the power delivered to the EV battery is:

$$P_L = R_L \left(\frac{M|I_1|}{L_2}\right)^2 \quad (3.10)$$

By substitution from equations (3.1) and (3.8), the following load power equation is reached:

$$P_L = R_L {I_1}^2 \left[\frac{1}{2(0.25 + ln\frac{d_1}{a})} ln \frac{\sqrt{h^2+(x+d_2)^2}\sqrt{h^2+(d_1-x)^2}}{\sqrt{h^2+x^2}\sqrt{h^2+(x+d_2-d_1)^2}}\right]^2 \quad (3.11)$$

Where P_L is the received power by the load, I_1 is the transmitter inductor current, R_L is the load resistance, h is the separation distance between coils, x is the displacement, d_1 & d_2 are the diameters of the coils, and a is the radius of the coil wire.

The above equation was plotted against displacement x once, and against the height h another time, to observe the behavior of the received power against the increase in displacement or height. The other constants were taken as follows: transmitter coil diameter = 1 meter, receiver coil diameter = 30 cm, load = 10 Ohms, radius of the wire = 0.5 cm, transmitter inductor current = 25 A. The plots achieved are shown in Figures 3.6 and 3.7.

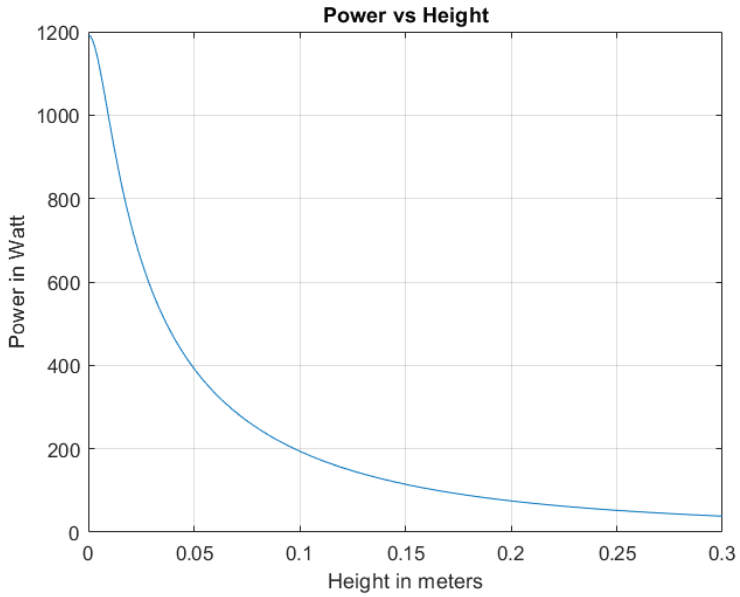

Figure 3.6: Delivered power vs. distance between transmitting and receiving coils.

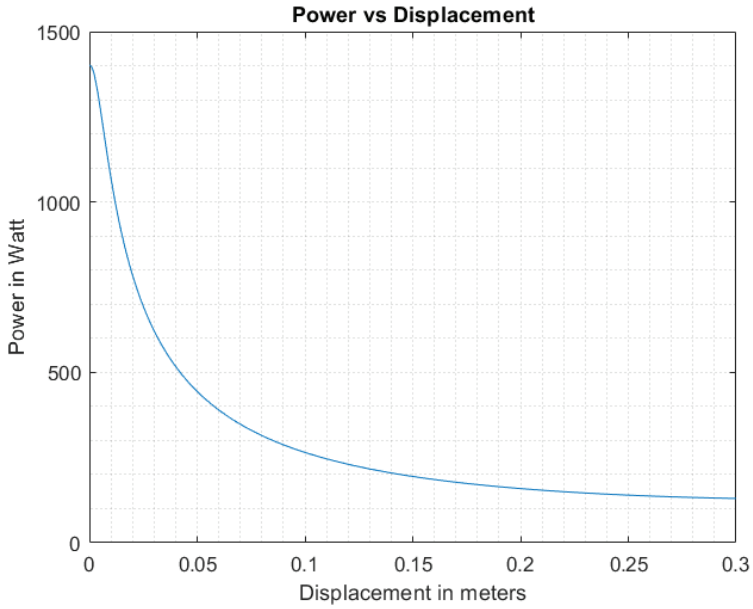

Figure 3.7: Delivered power vs. displacement between the centers of transmitting and receiving coils.

3.3. Coil Weight Calculation Formula

The next step was to formulate an equation to get the weight of the coils. The objective of this part is to ensure the coils' weights are reasonable. The coil weight

clearly reflects on its price, where the material price plays the major role in the entire coil price. The first step of calculating the weight is to get the length of the coil, which can then be converted to a volume, and thus converted into weight. The length *l* of any spiral coil is calculated as follows:

$$l = \int_{\theta_1}^{\theta_2} \sqrt{r^2 + (\frac{dr}{d\theta})^2}\, d\theta \qquad (3.\ 12)$$

Where *l* is the length of the coil wire, θ is the rotating angle as shown in Figure 3.8, θ_1 = 0 and $\theta_2 = 2\pi N$ are the start and end angles of the coil, *N* is the number of turns, and *r* is the distance from the origin. An Archimedean Spiral has general equation in polar coordinates:

$$r = c + b\theta \qquad (3.\ 13)$$

Where *c* is the starting radius of the coil, as shown in Figure 3.9, and $2\pi b$ is the change in radius, as shown in Figure 3.10.

The coil weight (*w*) can then be simply calculated as copper density (8.96 g/cm^3) multiplied by the coil wire volume, as follows:

$$w = 8.96 \times \pi a^2 l \qquad (3.\ 14)$$

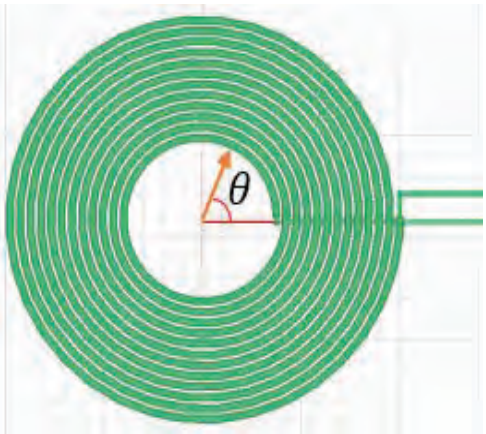

Figure 3.8: Angle of rotation.

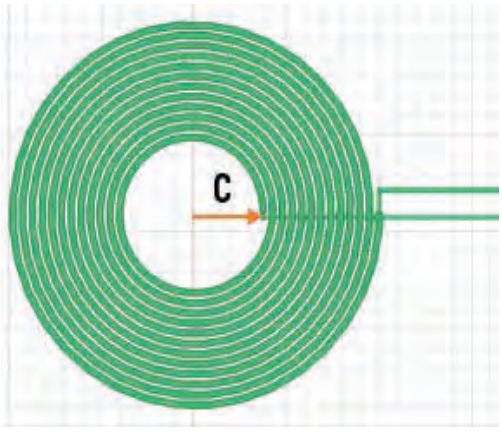

Figure 3.9: Coil's starting radius.

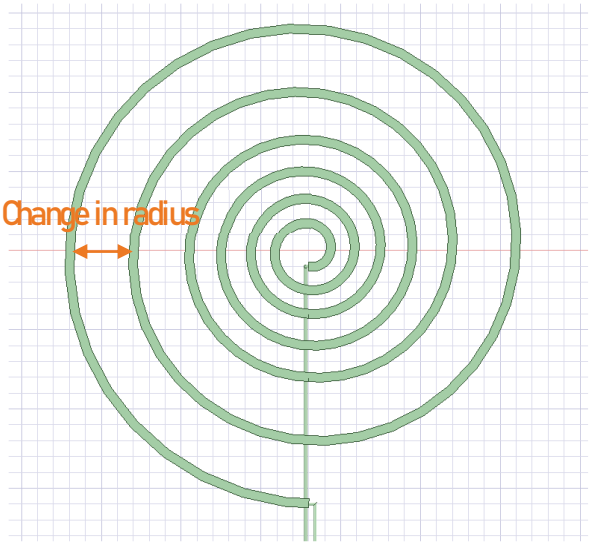

Figure 3.10: Coil's change in radius.

The objective function is to maximize P_L(a, d_1, d_2, h, x) or minimize 1/P_L(a, d_1, d_2, h, x), for every:

$$0.4m \leq d_1 \leq 2m$$

$$0.1m \leq d_2 \leq 1.3m$$

$$0.002m \leq a \leq 0.05m$$

$$0 \leq w \leq 30 \text{ Kg}$$

$$0 \leq a \leq \sqrt{\frac{30000}{8.96 * \pi l}}$$

$$h \in [0.04,\ 0.4]m$$

$$x \in [0,\ 0.3]m$$

$$I_1 = 25\ A$$

Where l is the coil wire length, which is a function of the coil starting radius (b) and the change in radius (CHR), and:

$$d_1 = b_{transmitter} + N_{transmitter} \times CHR_{transmitter} \quad (3.\ 15)$$

$$d_2 = b_{receiver} + N_{receiver} \times CHR_{receiver} \quad (3.\ 16)$$

3.4. Optimization Using MATLAB

MATLAB provides a powerful optimization toolbox, which offers several types of solvers with different algorithms. Solvers and algorithms are chosen depending on the nature of the optimization problem. In this research, two solvers will be used; fmincon, and genetic algorithm. Fmincon is a solver that finds the minimum of a constrained nonlinear multivariable function. For that, the objective function should be - P_L or $1/P_L$, where the maximum P_L can be found through minimizing the objective function. Fmincon uses different algorithms such as interior point, SQP, and active set. Interior point is usually the most accurate. SQP stands for Sequential Geometric Programming. It replaces the objective function with a quadratic approximation of the model, and replaces the constraints with linear approximations. Active set takes large steps and therefore it is the fastest. Genetic algorithm is based on searching for the global minimum of the function, therefore $1/P_L$ should be used as the fitness function.

3.4.1. Fmincon with interior point algorithm. The usage of different solvers and algorithms here is just to ensure reaching the correct optimized quantities. Firstly, fmincon was used with the interior point algorithm. The objective function has to be written in a MATLAB function script, and then called in the optimization toolbox. The starting point of optimization has to be chosen for all variables, as well as the constraints, which are in the form of bounds in our case. Figure 3.11 shows the optimization outcomes in case of using fmincon with interior point algorithm to optimize the value of the receiver coil diameter, where the transmitter coil diameter is set at 1 meter, the receiver coil diameter is constrained between 0.3m and 1.1m.

3.4.2. Fmincon with SQP algorithm. Secondly, fmincon was used with the SQP algorithm. Figure 3.12 shows the optimization outcomes in case of using fmincon with SQP algorithm to optimize the values of the receiver coil diameter, with the same constraints mentioned in the previous part.

3.4.3. Fmincon with active set algorithm. Thirdly, fmincon was used with the active set algorithm. Figure 3.13 shows the optimization outcomes in case of using fmincon with active set algorithm.

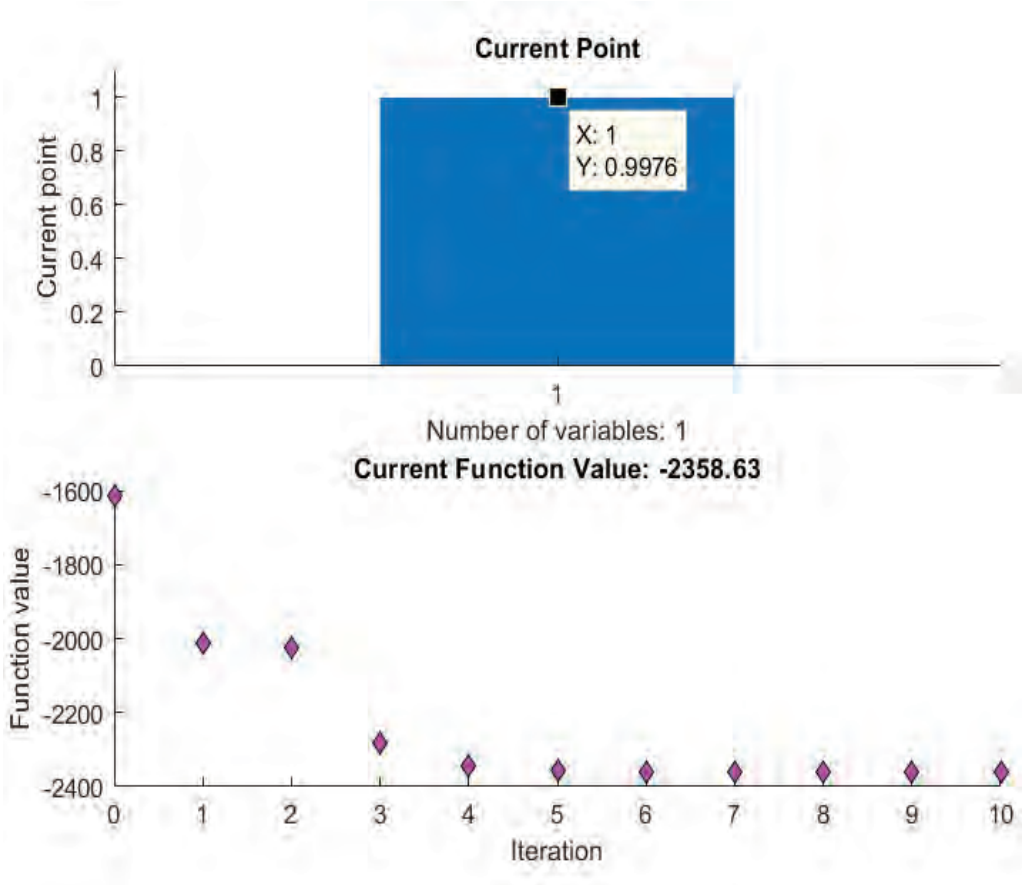

Figure 3.11: MATLAB optimization outcomes with fmincon interior point.

3.4.4. Genetic algorithm. The last type of solver used was genetic algorithm, which looks into the population of the data set, generates chromosomes, and uses the fitness function to pick random chromosomes. The chromosomes are then given weights using the roulette wheel. Crossover and mutation are done on the picked chromosomes to generate the next generation of chromosomes, and the process is repeated till reaching the minimum value of the objective function. Figure 3.14 shows the optimization outcomes in case of using genetic algorithm with the same constraints used in case of using the fmincon solver. As we're optimizing one variable here, 50 points for the population size should be enough, where 50 points is usually enough when optimizing 5 or fewer variables. However, the population size was chosen to be 100 points for more accuracy. For reproduction, default values were used, where the elite count was set to be 5% of population size, while the crossover fraction was set to 0.8.

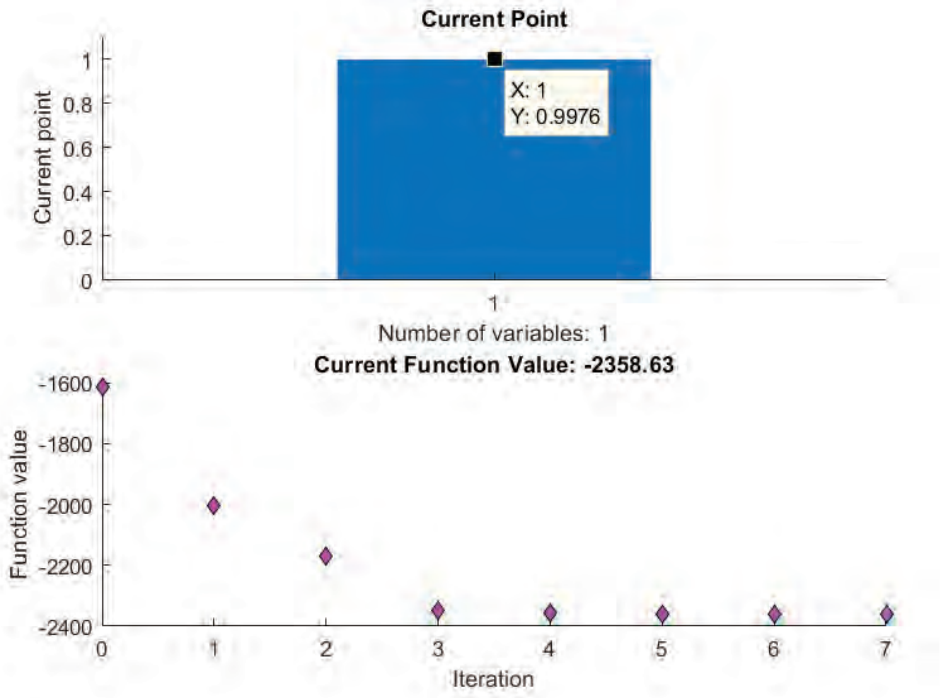

Figure 3.12: MATLAB optimization outcomes with fmincon SQP.

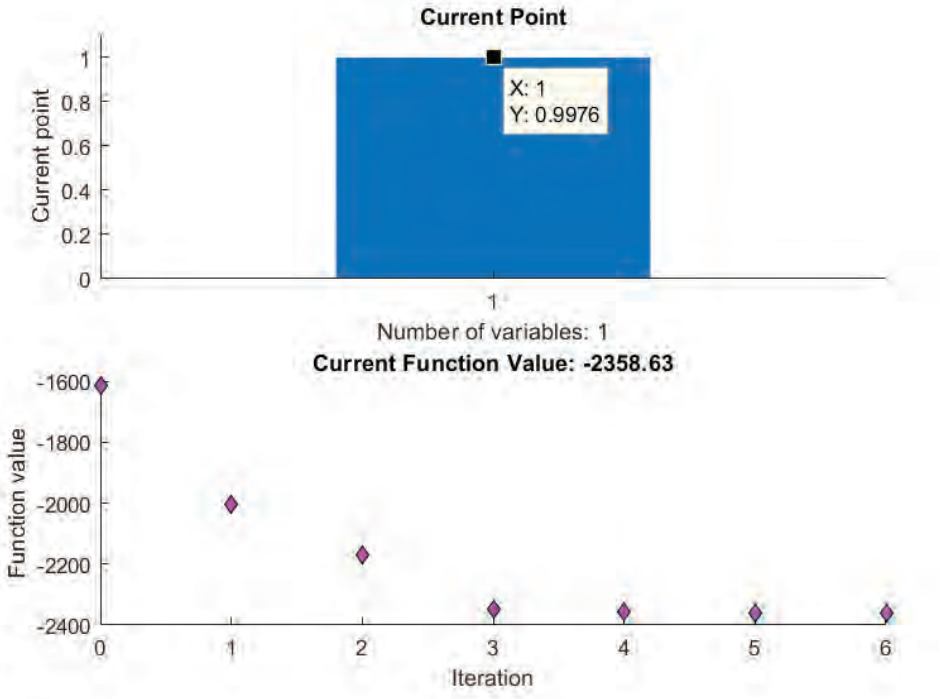

Figure 3.13: MATLAB optimization outcomes with fmincon active set.

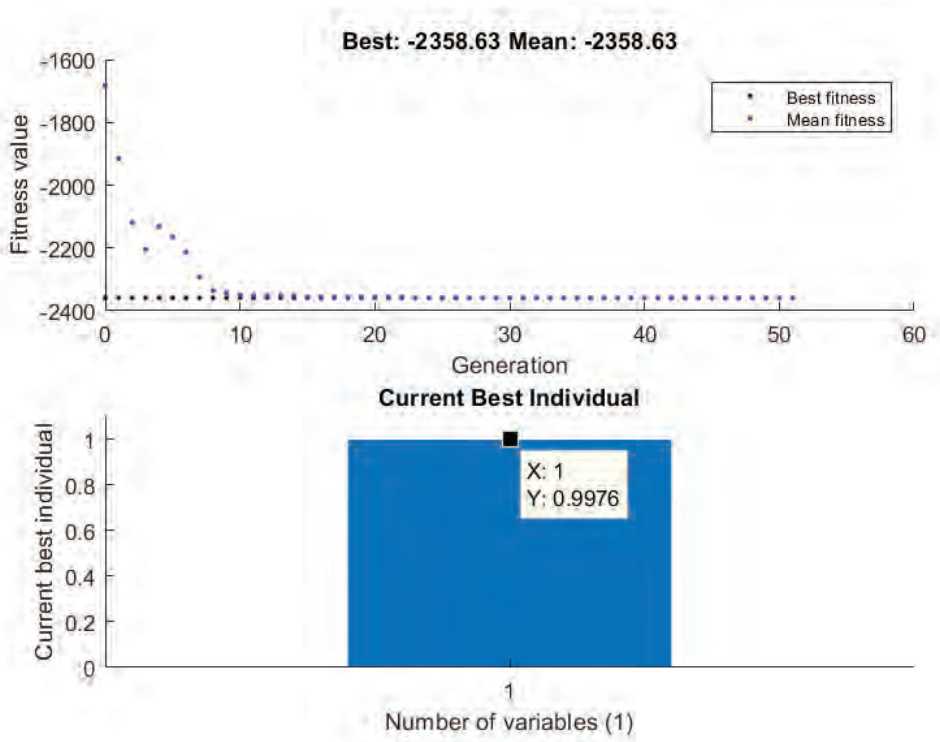

Figure 3.14: MATLAB optimization outcomes with Genetic Algorithm.

3.5. Optimization Outcome Trends

The bounds were practically chosen to match reality. For instance, the diameter of the transmitter coil has to be limited to the width of the parking slot. On the other hand, the receiver coil has to be of a reasonable diameter compared to the vehicle's width. As a result, the upper constrain of the transmitter coil is always expected to be higher than that of the receiver coil, as the parking slot width should always be greater than the vehicle's width. A large number of optimization cycles was done to test numerous different cases, where the constrained variables were varied. It was clearly noticed that the optimization outcomes have some trends. One of the most important observed trends is that the transmitter coil and receiver coil diameters try to match each other, or get as close as possible depending on the constraints. The receiver coil diameter tries to maximize itself as much as possible, or as much as the constraints permit, but not higher than the transmitter coil diameter. The wire radius always tries to maximize itself as that will result in higher power. However, this will be constrained with the coil weight, as well as its price. Tables 3.1, 3.2, and 3.3 show a summary of the optimization cycles done, and the calculated output power.

Table 3.1: Optimization of the transmitting coil diameter.

Parameter	Run 1	Run 2	Run 3
d_2 (m)	1.3	1.1	1
a (cm)	1	1	1
h (m)	0.1	0.1	0.1
x_1	0	0	0
I (A)	25	25	25
R_L (Ω)	10	10	10
d_1 min limit (m)	1	1	1
d_1 max limit (m)	3	3	3
d_1 optimized (m)	1.308	1.109	1.012
$1/P_L$	0.0006347	0.0006784	0.0007068
P_L	1575.54	1474.06	1414.83

Table 3.2: Optimization of the transmitting and receiving coils diameters.

Parameter	Run 1	Run 2	Run 3	Run 4	Run 5	Run 6
a (cm)	1	1	1	1	1	1
h (m)	0.1	0.1	0.1	0.1	0.06	0.04
x_1 (m)	0	0	0.1	0.1	0.2	0.2
I (A)	25	25	25	25	25	25
R_L (Ω)	10	10	10	10	10	10
d_1 min limit (m)	0.5	0.5	0.5	0.5	0.5	0.5
d_1 max limit (m)	1.5	1	1	2	2	2
d_1 optimized (m)	1.5	1	1	1.3	1.4	1.4
d_2 min limit (m)	0.7	0.8	0.8	0.5	0.5	0.5
d_2 max limit (m)	1.5	1.5	1.5	1.2	1.2	1.2
d_2 optimized (m)	1.5	1	0.9	1.2	1.2	1.2
$1/P_L$	0.0006	0.00071	0.0008	0.00073	0.00068	0.00057
P_L (W)	1658.48	1410.92	1200.5	1367.62	1478.68	1747.23

Table 3.3: Optimization of the transmitting coil diameter and the wire radius.

Parameter	Run 1	Run 2	Run 3	Run 4
d_1 (m)	1.4	1.4	1.2	1.3
h (m)	0.04	0.04	0.02	0.03
x_1 (m)	0	0	0	0
d_2 min limit (m)	0.5	0.5	0.8	0.7
d_2 max limit (m)	1.2	1.6	1.2	1.4
d_2 optimized (m)	1.2	1.4	1.2	1.3
a min limit (cm)	0.5	0.5	0.5	0.5
a max limit (cm)	3	5	2	4
a optimized (cm)	3	3	1.9	3.9
$1/P_L$	0.0003497	0.0002121	0.0002747	0.0001579
P_L (W)	2859.42	4713.78	3640.33	6333.12

3.6. Analytical Optimization

Analytical optimization was done to verify the optimization done using MATLAB optimization toolbox. The main purpose of verification is to mathematically prove the trends observed throughout section 3.4.

3.6.1. Analytical optimization procedure. Analytical optimization will be done on the case where the receiver coil diameter d_2 is the only variable. In other words, the power received by the load will be maximized through optimizing the receiver coil diameter. The equation of the power received by the load was obtained earlier, as shown below.

$$P_L = R_L {I_1}^2 \left[\frac{1}{2(0.25+ln\frac{d_1}{a})} ln \frac{\sqrt{h^2+(x+d_2)^2}\sqrt{h^2+(d_1-x)^2}}{\sqrt{h^2+x^2}\sqrt{h^2+(x+d_2-d_1)^2}}\right]^2 \quad (3.\ 17)$$

For the case of having the receiver coil diameter d_2 as the only variable, we get:

$$P_L(d_2) = K\left[ln \frac{AxB}{C \times (D+(E+d_2)^2)}\right]^2 \quad (3.\ 18)$$

Where:

$$K = \frac{R_L {I_1}^2}{\left[4(0.25 + ln\frac{d_1}{a}\right]^2}$$

$$A = h^2 + (x + d_1)^2$$

$$B = h^2 + (d_1 - x)^2$$

$$C = h^2 + x^2$$

$$D = h^2$$

$$E = x - d_1$$

Furthermore:

$$P_L(d_2) = K[ln(A \times B) - ln(C(D + E^2 + 2Ed_2 + d_2^2)]^2 \quad (3.\ 19)$$

$$P_L(d_2) = K[ln(F) - ln(Q + Rd_2 + Cd_2^2)]^2 \quad (3.\ 20)$$

Where:

$$F = A \times B$$

$$Q = C(D + E^2)$$

$$R = 2 \times E \times C$$

Let:

$$Q + R\mathrm{d}_2 + Cd_2^2 = (d_2 + S)(d_2 + T) \quad (3.\ 21)$$

Therefore:

$$P_L(d_2) = K[ln(F) - ln(d_2 + S)(d_2 + T)]^2 \quad (3.\ 22)$$

$$P_L(d_2) = K[ln(F) - ln(d_2 + S) - ln(d_2 + T)]^2 \quad (3.\ 23)$$

Now by taking the derivative of $P_{L(d2)}$ with respect to d_2 we get:

$$\frac{dP_L(d_2)}{dd_2} = 2K[ln(F) - ln(d_2 + S) - ln(d_2 + T)]$$

$$-\frac{d}{dd_2}[ln(F) - ln(d_2 + S) - ln(d_2 + T)] \quad (3.\ 24)$$

$$\frac{dP_L(d_2)}{dd_2} = 2K[ln(F) - ln(d_2 + S) - ln(d_2 + T)]\left[\frac{-1}{d_2+S} - \frac{1}{d_2+T}\right] \quad (3.\ 25)$$

Therefore by replacing the constants back, we get:

$$\frac{dP_L(d_2)}{dd_2} = \frac{R_L {I_1}^2}{8\left[(0.25 + ln\frac{d_1}{a}\right]^2}[ln[(h^2 + (x + d_1)^2)(h^2 + (d_1 - x)^2)]$$

$$- ln(d_2 + S) - ln(d_2 + T)]\left[\frac{-1}{d_2+S} - \frac{1}{d_2+T}\right] \quad (3.\ 26)$$

3.6.2. Power derivative zero crossing. The next step was to plot this derivative function against d_2 using MATLAB, and check the point at which the derivative is equal to zero. In other words, check the value of d_2 at which the derivative is equal to 0. The value of d_1 was chosen to be 0.8 m, 1 m, and 1.2 m. Figures 3.15, 3.16, and 3.17 show the plot of the derivative against d_2 at the 3 different values of d_1. The plots clearly verifies the trend stated earlier, which indicates that d_2 is maximized with a ceiling of d_1. The two additional zero crossings which appear in Figure 3.19 aren't considered optimized points in our case. The reason for ignoring the first of the 2 additional zero crossings is that it appears at a receiver coil diameter of 15 cm, which translates into less than 1 coil turn, as the coil wire radius here was specified as 3 cm. The reason for

ignoring the second of the 2 additional zero crossings is that it appears at a receiver diameter of 1.45m, which is beyond the maximum specified limit for the receiver diameter, as that exceeds the width of an EV.

3.6.3. Double checking the zero crossing of the derivative function. One last step is to further verify the work done in the optimization by hand section. The terms of the derivative function shown in equation (3.26) were investigated to list down the conditions that cause any of them to be a zero term. The first condition is having R_L equal to zero, which is infeasible as it indicates a short circuit on the battery. The second condition is having I_1 equal to zero, which is also infeasible as it indicates that there is no current provided by the source. The third condition is having:

$$\frac{-1}{d_2+S} = \frac{1}{d_2+T} \tag{3. 27}$$

Equations (3.28) till (3.36) show that this condition is only feasible if there's absolutely no overlap between the transmitter and receiver coils, a case which almost provides no WPT.

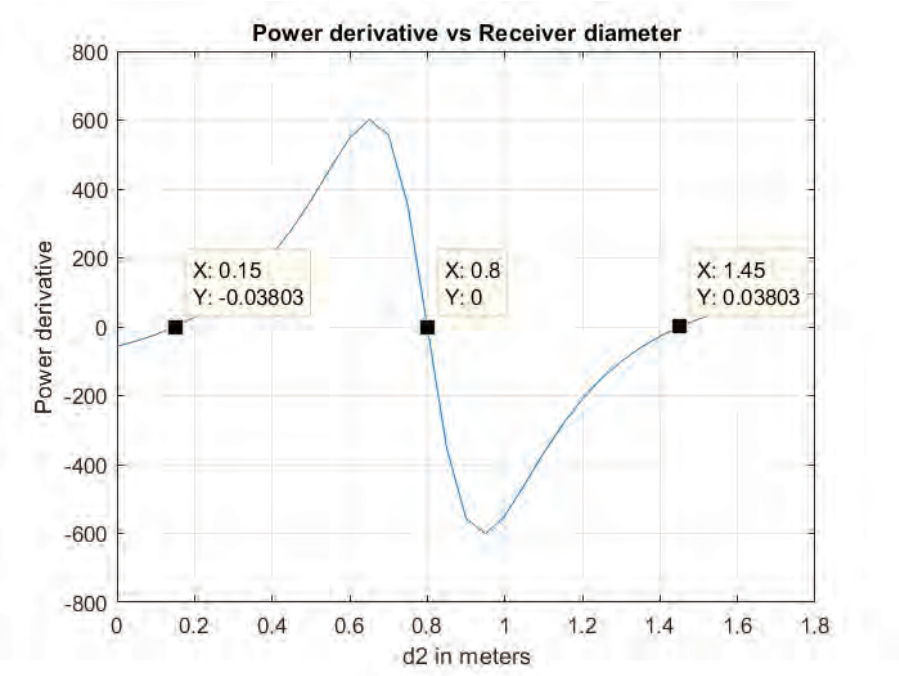

Figure 3.15: Power derivative vs. receiver diameter at transmitter diameter of 0.8 meter.

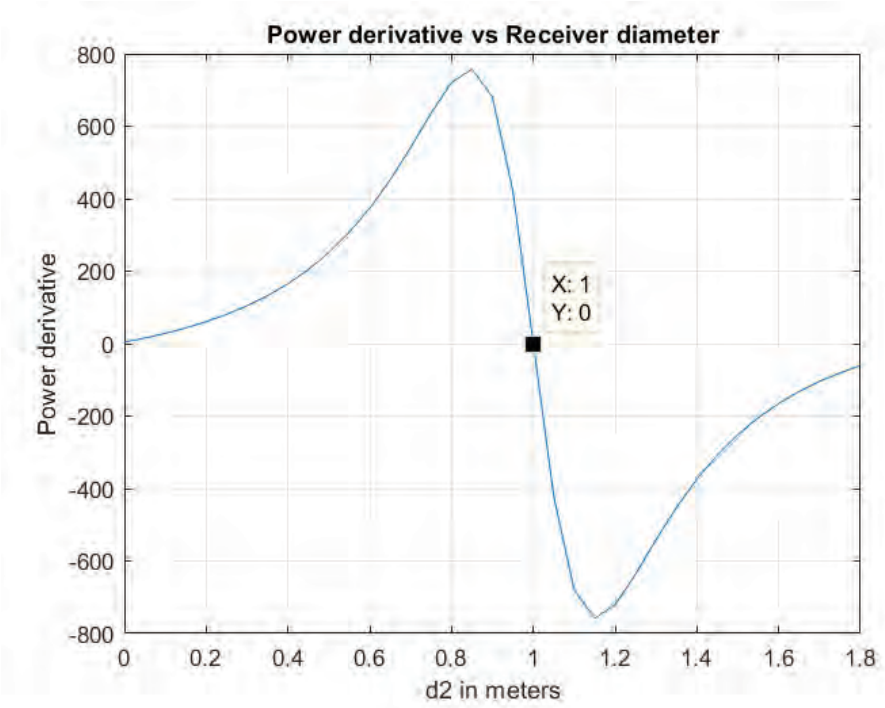

Figure 3.16: Power derivative vs. receiver diameter at transmitter diameter of 1 meter.

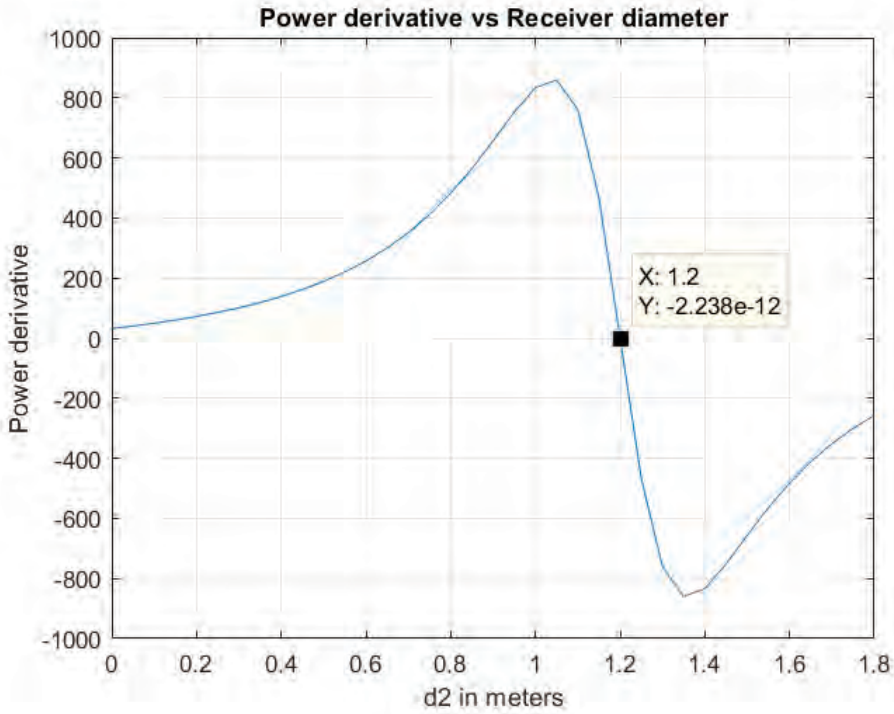

Figure 3.17: Power derivative vs. receiver diameter at transmitter diameter of 1.2 meter.

Since:

$$-d_2 - T = d_2 + S \tag{3. 28}$$

Therefore:

$$2d_2 = -(T + S) \tag{3. 29}$$

And since:

$$Q + R\mathrm{d}_2 + Cd_2^2 = (d_2 + S)(d_2 + T) \tag{3. 30}$$

Therefore:

$$S = \frac{\frac{-R}{C} + \sqrt{\frac{R^2}{C} - 4\frac{Q}{C}}}{2} \tag{3. 31}$$

And:

$$T = \frac{\frac{-R}{C} - \sqrt{\frac{R^2}{C} - 4\frac{Q}{C}}}{2} \tag{32)}$$

Therefore:

$$T + S = -\frac{R}{2C} \tag{3. 33}$$

$$2d_2 = \frac{R}{2C} \tag{3. 34}$$

$$2d_2 = \frac{2(x - d_1)(h^2 + x^2)}{2(h^2 + x^2)} \tag{3. 35}$$

$$2d_2 = x - d_1 \tag{3. 36}$$

Equation (3.26) can only be fulfilled if there's zero overlap between the transmitter and receiver coils. The fourth and last condition is when:

$$ln[(h^2 + (x + d_1)^2)(h^2 + (d_1 - x)^2)] \ = ln(d_2 + S) + ln(d_2 + T) \tag{3. 37}$$

$$(h^2 + (x + d_1)^2)(\, h^2 + (d_1 - x)^2) = (d_2 + S)(d_2 + T) \tag{3. 38}$$

Therefore equation (3.39) can be considered as a constraint, where:

$$(h^2 + (x + d_1)^2)(\, h^2 + (d_1 - x)^2) \neq (d_2 + S)(d_2 + T) \qquad (3.\ 39)$$

3.7. ANSYS Maxwell

Simulation is indeed a very important step in this research. The main source of importance generates from the fact that simulation will double check the values achieved from optimization, will help us better forecast the behavior and performance of the wireless power transfer system, as well as that it might help us reduce the cost or improve the full system efficiency.

3.7.1. ANSYS Maxwell features and capabilities. ANSYS Maxwell is a powerful electromagnetic simulator which uses the accurate finite element method to solve electromagnetic fields. Once you get to know how to use the software, it becomes easy to simulate different scenarios of wireless power transfer where you can specify different geometries, different materials, and different types of outputs. A key feature of the software is its ability of automatic mesh generation. The software uses an advanced meshing technique that reduces the required memory for simulation, and removes complexity during the analysis process. Figure 3.18 shows an example of how automatic meshing looks like.

As for the solution types, ANSYS Maxwell offers several options such as the AC electromagnetic, the magnetostatic, and the electric field solution type. AC electromagnetic is used for systems affected by skin effect and eddy currents. Magnetostatic is used for nonlinear systems, and it automatically provides an equivalent

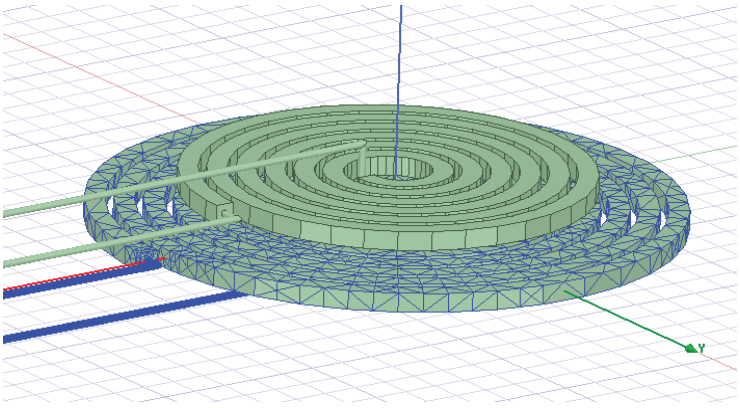

Figure 3.18: ANSYS Maxwell automatic meshing

circuit model. Electric field solution type is used for transient analysis, and it also provides an equivalent circuit model.

The inputs to ANSYS Maxwell can be briefed as: the wire cross section dimensions, the coil starting radius, the change in radius, the coil number of turns, the misalignment between the centers of the 2 coils, the separating distance between the 2 coils, the material of the coil wire, the material of the ambient, the excitation type whether is it current or voltage excitation, the amount of excitation used, the dimensions of the simulating environment, the solution type, and the number of segments each coil is divided into, which contributes to the accuracy and speed of simulation.

3.7.2. ANSYS Maxwell simulation procedure. This part is going to discuss the different case studies taken in our simulation stage. The main differences between the case scenarios can be briefed as: the presence or absence of misalignment between the centers of the coils, and the nature of change in radius, weather it is constant or variable. Change in radius is the difference between the previous turn's radius and the current turn's radius. This change can be constant throughout all turns of the coil, or it can be varying. It was noticed through simulation that the parameter of change in radius can clearly affect the efficiency of the system, therefore studying its effect was taken into consideration. The change in radius can be constant in both coils, variable in both coils, or constant in one coil and variable in the other.

Having a variable change in radius in the receiver coil is more beneficial as it will contribute in reducing the weight of the coil, which can contribute slightly in the EV's driving range. Moreover, this variable change in radius can be utilized to reduce the amount of material used, and consequently reducing the coil manufacturing cost and final price.

If the difference between the previous turn's radius and the current turn's radius is increasing as the number of turns increase, then it is said that the change in radius is having an increasing variation. In contrary, if this difference is decreasing as the turns increase, it is said that the change in radius is having a decreasing variation. Having a change in radius with increasing variation contributes in reducing the coil weight and the amount of material used, therefore reducing the consumed power and the coil price. However, coils with decreasing variation were also simulated to check their power

transfer characteristics, but were found to have less power transferred when compared to coils having an increasing variation. Therefore the decreasing variation was excluded from this research's case studies.

3.8. Case Studies Designed on ANSYS Maxwell

Nine case studies, divided into 3 categories, were designed and tested on ANSYS Maxwell. Category A contains 3 designs, having a constant change in radius in both coils, with different misalignments between the centers of the coils. The first of which has a perfect alignment, the second has a misalignment of 10% of its radius, while the third has a misalignment of 20% of its radius. The same sequence of misalignment goes for the other 2 categories, where category B is characterized by having a variable change in radius in both coils, while category C has a variable change in radius in the receiver coil only.

3.8.1. Category A: constant change in radius in both coils. The parameters used as inputs for category A Maxwell simulation, are shown in Table 3.4. The transmitter's and receiver's diameters are both 1 meter. Transmitter coil is colored in grey, while the receiver coil is colored in blue. Case study 1 has a perfect alignment between its coils. Figures 3.19, 3.20, and 3.21 show the coils implemented on ANSYS Maxwell for case study 1. Case study 2 adds a 5 cm misalignment to case study 1, that's 10% of the coils' radii. Figure 3.22 shows the coils implemented on ANSYS Maxwell for case study 2. Finally, case study 3 adds a 10 cm misalignment to case study 1, that's 20% of the coils' radii. Figure 3.23 shows the coils implemented on ANSYS Maxwell for case study 3.

3.8.2. Category B: variable change in radius in both coils. The parameters used as inputs for category B Maxwell simulation, are shown in Table 3.5. The transmitter's and receiver's diameters are both 1 meter. Transmitter coil is colored in grey, while the receiver coil is colored in blue. Case study 4 has a perfect alignment between its coils. Figures 3.24 and 3.25 show the coils implemented on ANSYS Maxwell for case study 4. Case study 5 adds a 5 cm misalignment to case study 4, that's 10% of the coils' radii. Figures 3.26 and 3.27 show the coils implemented on ANSYS Maxwell for case study 5. Finally, case study 6 adds a 10 cm misalignment to case study

4, that's 20% of the coils' radii. Figure 3.28 shows the coils implemented on ANSYS Maxwell for case study 6.

Table 3.4: ANSYS Maxwell simulation parameters.

Transmitter number of turns ($N_{transmitter}$)	9
Transmitter starting radius ($c_{transmitter}$)	10 cm
Transmitter radius change ($CHR_{transmitter}$)	5 cm
Receiver number of turns ($N_{receiver}$)	9
Receiver starting radius ($c_{receiver}$)	10 cm
Receiver radius change ($CHR_{receiver}$)	5 cm
Distance between coils (h)	9 cm

Table 3.5: ANSYS Maxwell simulation parameters.

Transmitter number of turns ($N_{transmitter}$)	6
Transmitter starting radius ($c_{transmitter}$)	10 cm
Transmitter radius change ($CHR_{transmitter}$)	Inner 2 turns – 4 cm Middle 2 turns – 7 cm Outer 2 turns – 10 cm
Receiver number of turns ($N_{receiver}$)	6
Receiver starting radius ($c_{receiver}$)	10 cm
Receiver radius change ($CHR_{receiver}$)	Inner 2 turns – 4 cm Middle 2 turns – 7 cm Outer 2 turns – 10 cm
Distance between coils (h)	9 cm

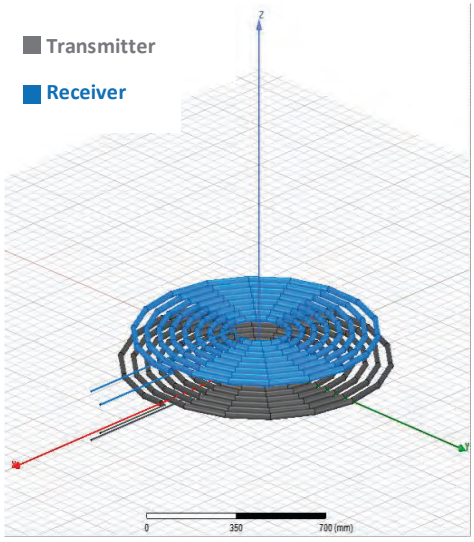

Figure 3.19: Transmitting and receiving coils in ANSYS Maxwell

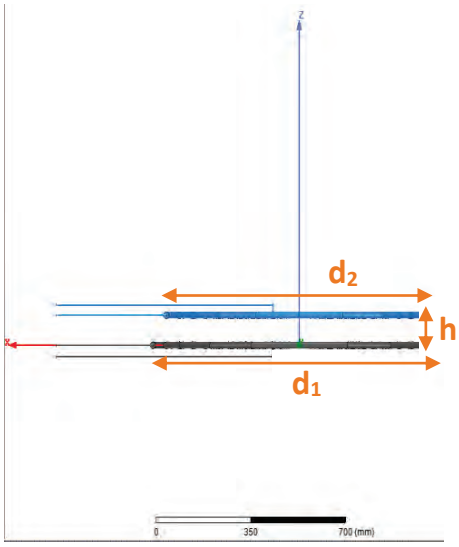

Figure 3.20: Side view of the coils on Maxwell

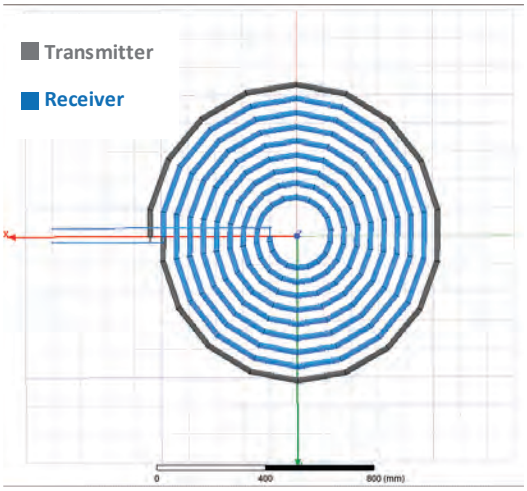

Figure 3.21: Top view of the coils on Maxwell.

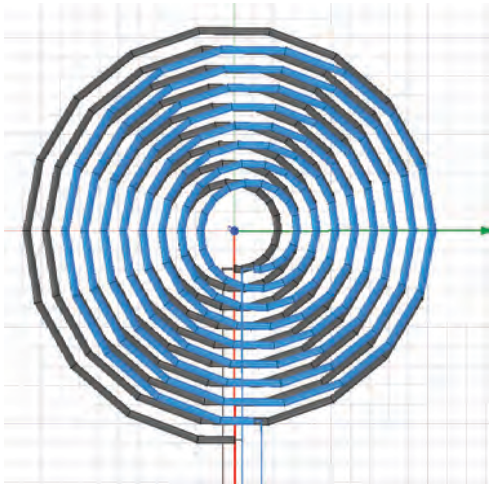

Figure 3.22: Top view of the coils on Maxwell.

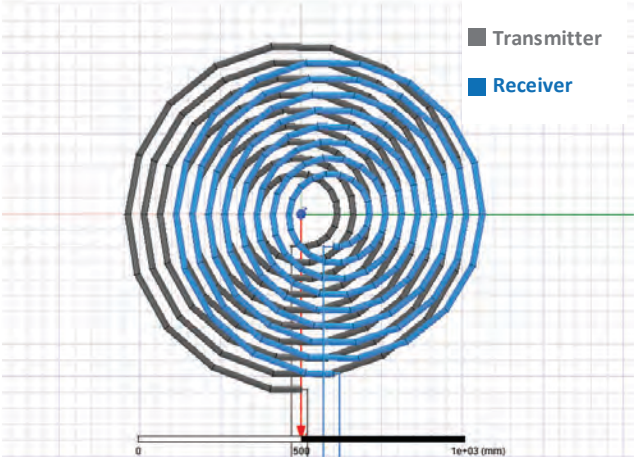

Figure 3.23: Top view of the coils on Maxwell.

3.8.3. Category C: variable change in radius in receiver coil only. The parameters used as inputs for category C Maxwell simulation, are shown in Table 3.6. The transmitter's and receiver's diameters are both 1 meter. Transmitter coil is colored in grey, while the receiver coil is colored in blue. Case study 7 has a perfect alignment between its coils. Figures 3.29 and 3.30 show the coils implemented on ANSYS Maxwell for case study 7. Case study 8 adds a 5 cm misalignment to case study 7, that's 10% of the coils' radii. Figures 3.31 and 3.32 show the coils implemented on ANSYS Maxwell for case study 8. Finally, case study 9 adds a 10 cm misalignment to case study

7, that's 20% of the coils' radii. Figures 3.33 and 3.34 show the coils implemented on ANSYS Maxwell for case study 9.

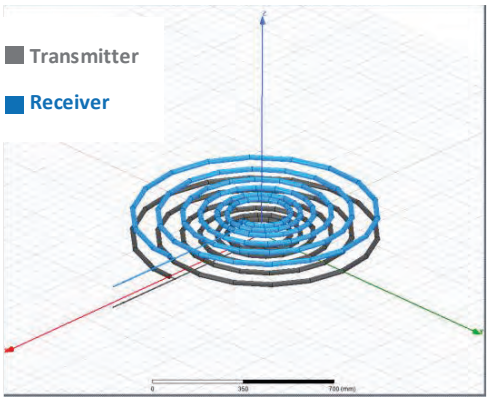

Figure 3.24: Transmitting and receiving coils with a variable change in radius.

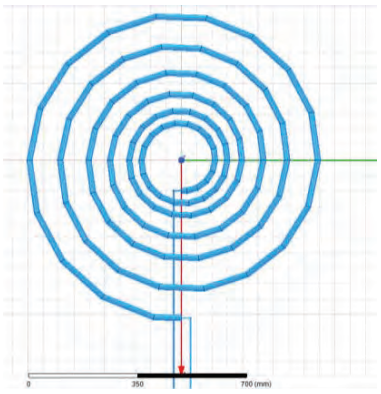

Figure 3.25: Top view with a variable change in radius.

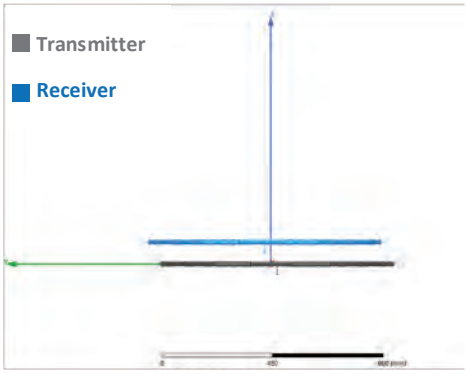

Figure 3.26: Variable change in radius in both coils and a 10% misalignment.

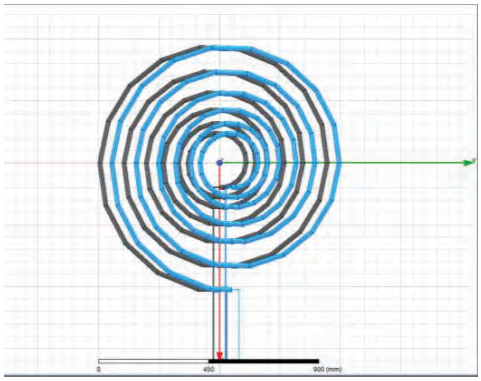

Figure 3.27: Top view with variable change in radius in both coils and a 10% misalignment.

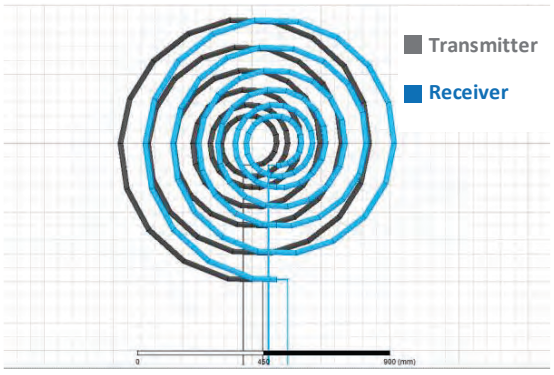

Figure 3.28: Top view of the coils on Maxwell.

Table 3.6: ANSYS Maxwell simulation parameters.

Transmitter number of turns ($N_{transmitter}$)	9
Transmitter starting radius ($c_{transmitter}$)	10 cm
Transmitter radius change ($CHR_{transmitter}$)	5 cm
Receiver number of turns ($N_{receiver}$)	6
Receiver starting radius ($c_{receiver}$)	8 cm
Receiver radius change ($CHR_{receiver}$)	Inner 2 turns – 4 cm Middle 2 turns – 7 cm Outer 2 turns – 10 cm
Distance between coils (h)	9 cm

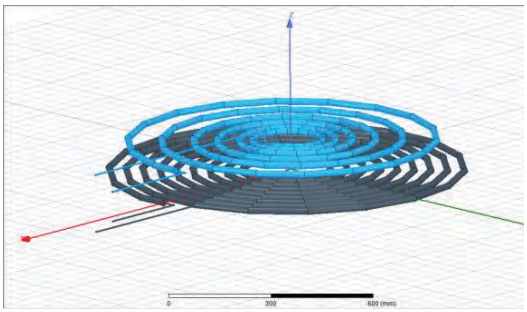

Figure 3.29: Receiving coil of a variable change in radius and transmitting coil of a constant change in radius.

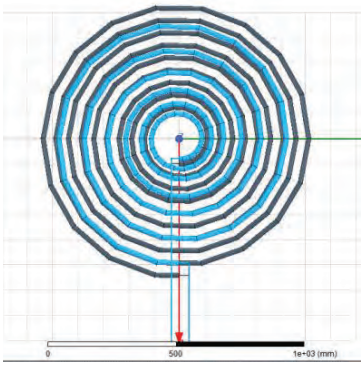

Figure 3.30: Top view of the receiving coil of a variable change in radius and transmitting coil of a constant change in radius.

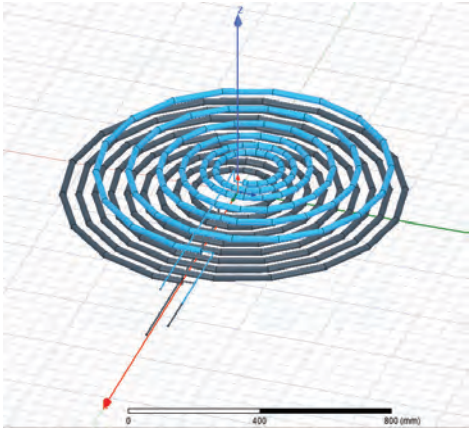

Figure 3.31: Transmitting and receiving coils with a variable change in radius and a 10% misalignment.

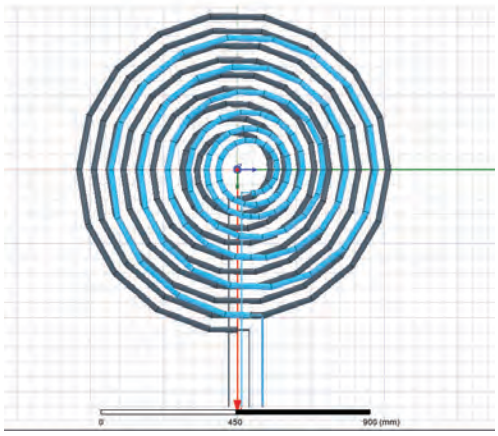

Figure 3.32: Top view with a variable change in radius and a 10% misalignment.

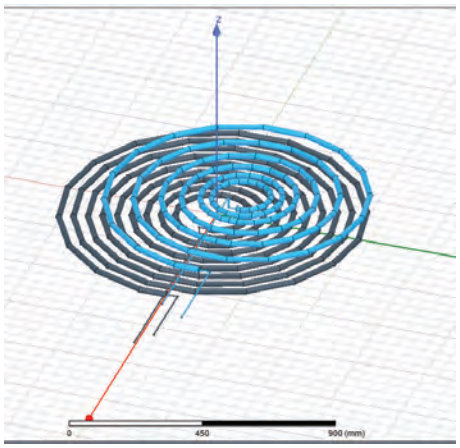

Figure 3.33: Transmitting and receiving coils with a variable change in radius and a 20% misalignment.

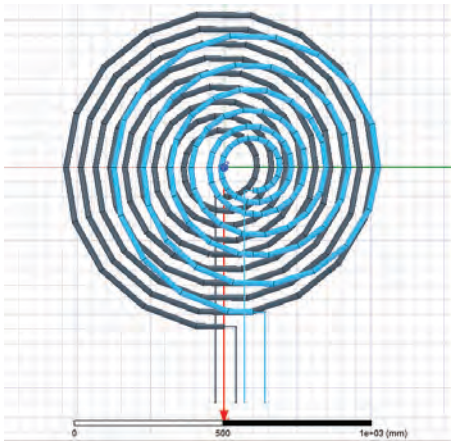

Figure 3.34: Top view with a variable change in radius and a 20% misalignment.

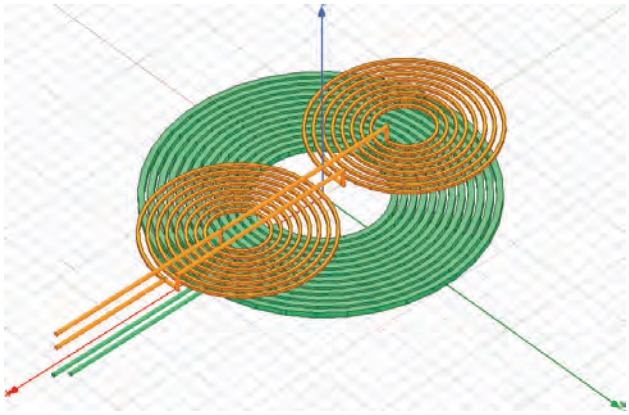

Figure 3.35: Double receiving coils designed using ANSYS Maxwell.

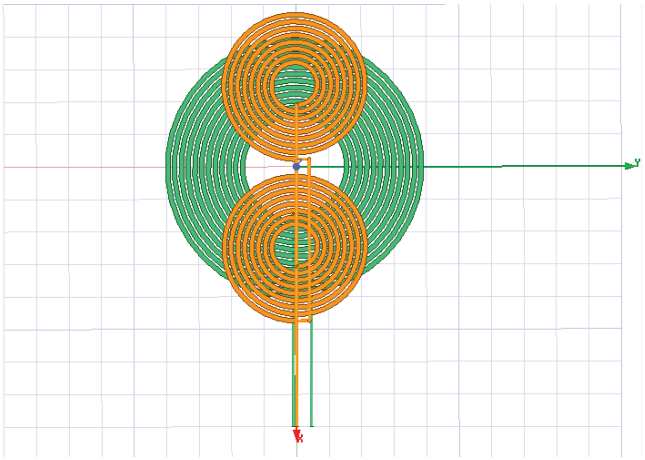

Figure 3.36: Top view of double receiving coils designed using ANSYS Maxwell.

3.8.4. Case study - double receivers. An ANSYS Maxwell model was created to simulate a WPT system having one transmitting coil two receiving coils connected in parallel. The main objective was to check if double receivers will have higher power transfer efficiency. Figures 3.35 and 3.36 show the trimetric and top views respectively.

3.9. ANSYS Simplorer

ANSYS Simplorer is another powerful platform that ANSYS provides, specifically for the aim of simulating system-level prototypes and models. ANSYS Maxwell was designed to provide an equivalent circuit for the model, which can be used as a part of the full system implemented on Simplorer.

3.9.1. ANSYS Simplorer features and capabilities. Simplorer enables the combination of accurate models with complex circuits, and therefore verifying and optimizing the system's performance. In magnetic resonance WPT, the amount of transferred power depends on the electrical characteristics of both the source and the load. The transmitting and receiving coils should be tuned to resonate at the same frequency. This can be achieved through adding some electrical components, in addition to the design of the coils, in terms of their geometry. ANSYS Simplorer makes it possible to simulate such a system, as it has the ability to solve electrical and magnetic fields at the same time, where it can account for the electrical components in the circuit, as well as the coils' geometry.

3.9.2. ANSYS Simplorer simulation. The full circuit is implemented on ANSYS Simplorer, as shown in Figure 3.37. Literature shows that this equivalent circuit can be used for simulation instead of the actual WPT circuit, to simplify the rectifier part which should precede the battery [36]. The primary side consists of an AC voltage source, a resistance, a capacitor C_T connected in series with the transmitter coil to ensure maximum current delivered to the transmitter, and the transmitter coil. The secondary side starts with the receiving coil, followed by a capacitor C_R connected in parallel to ensure maximum voltage drop on the car's battery, and the car's battery impedance and the rectifier impedance as seen by the receiver coil, represented by a resistance R_{eq}, in addition to a series capacitance C_{eq}.

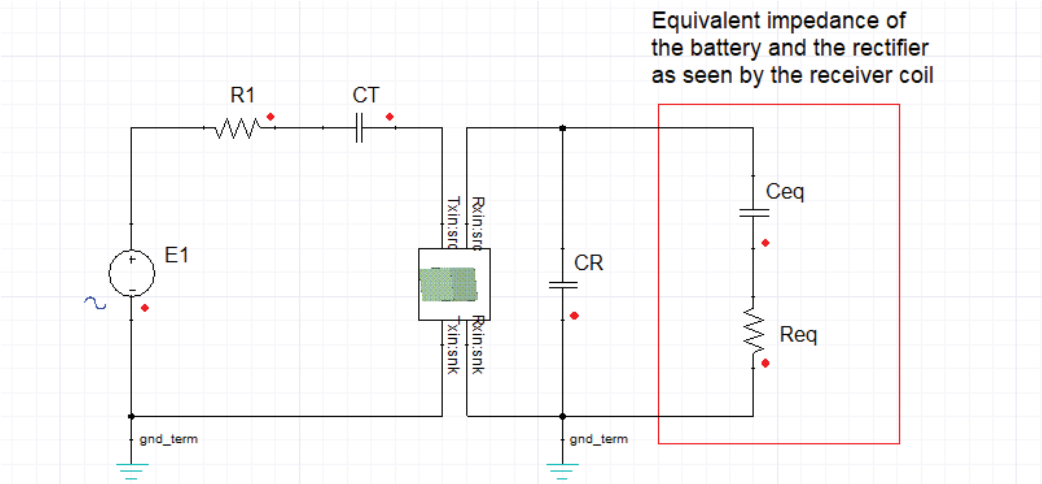

Figure 3.37: Full circuit implementation on ANSYS Simplorer.

3.9.3. Resonance. The values for both capacitors were chosen to achieve resonance, using equation (3.40). However, the resonance is expect to occur at a higher frequency than the designed resonance frequency. The resonance frequency shift is mainly due to the magnetic inductance. When a magnetic field is applied, magnetostrictive stress takes place. Magnetostrictive stress is a ferromagnetic materials property, which causes the material to expand or contract due to the applied magnetic field. This magnetostrictive stress induced an axial force which shifts the resonance frequency towards a higher value. A research done in China showed that the shift in resonance frequency is approximately linear with the increase in the applied magnetic field [37].

$$C = \frac{1}{L(2\pi f)^2} \qquad (3.\ 40)$$

A hundred kHz was chosen to be the designing resonance frequency for our simulations. Literature shows that the current used resonance frequency in EV's wireless charging ranges between 20 kHz and 2 MHz, with current ongoing theoretical research trying to reach 20 MHz [38]-[39] [40].

3.10. Relating Consumed Power to the Receiving Coil Weight

Researchers in University of Michigan studied the relation between customer needs and electric vehicle performance [41]. The effect of the receiving coil weight on

the electric vehicle's power consumption will be studied through the rules published in their research paper, as follows:

$$P = F_{tr} \times V \tag{3. 41}$$

$$F_{tr} = ma + F_{roll} + F_{AD} + F_g \tag{3. 42}$$

$$F_{roll} = m \times g \times C_1 \times V^2 \tag{3. 43}$$

$$F_{AD} = 0.5 \times \rho \times C_D \times A_F \times V^2 \tag{3. 44}$$

$$F_g = m \times g \times \sin\alpha \tag{3. 45}$$

Therefore,

$$P = [ma + m \times g \times C_1 \times V^2 + 0.5 \times \rho \times C_D \times A_F \times V^2 + m \times g \times \sin\alpha] \times V \tag{3. 46}$$

Where P is the power consumption (W), F_{tr} is the traction force (N), V is the vehicle velocity (m/s), m is the vehicle mass (kg), a is the acceleration (m/s^2), F_{roll} is the rolling resistance (N), F_{AD} is the aerodynamic drag (N), F_g is the grading resistance (N), g is the acceleration due to gravity (m/s^2), C_1 is the rolling resistance coefficient (s^2/m^2), ρ is the density of air (kg/m^3), C_D is the aerodynamic drag coefficient, A_F is the frontal area (m^2), and α is the grade angle.

3.11. Relation Between Battery's State of Charge and its Internal Impedance

One interesting topic to look at is the EV battery's state of charge (SOC). The battery's internal impedance may slightly change due to the variation in the SOC. The change in impedance can affect the resonance frequency, and therefore shift the power transfer efficiency peak to a frequency different from the operating frequency. If this occurs, the wireless power transfer would operate at a non-peak value. In other words, the wireless power transfer would not be optimized. For these reasons, it was essential to look into the relation between the battery's SOC and the resonance frequency.

3.11.1. Li-ion battery equivalent circuit model. To begin with, an accurate model of a usual Li-ion battery used in EVs was needed. Researchers have done some valuable work into that part. Figure 3.38 shows an equivalent circuit model for the Li-ion battery [42]. The battery's parameters in the model used are all dependent on the battery's SOC (x_1), which is a number between 0 and 1. Equations (3.47) till (3.52) show the relations used to calculate the values for the voltage source E_0, the resistances R_s, R_{ts}, and R_{tl}, as well as the capacitances C_{ts} and C_{tl}.

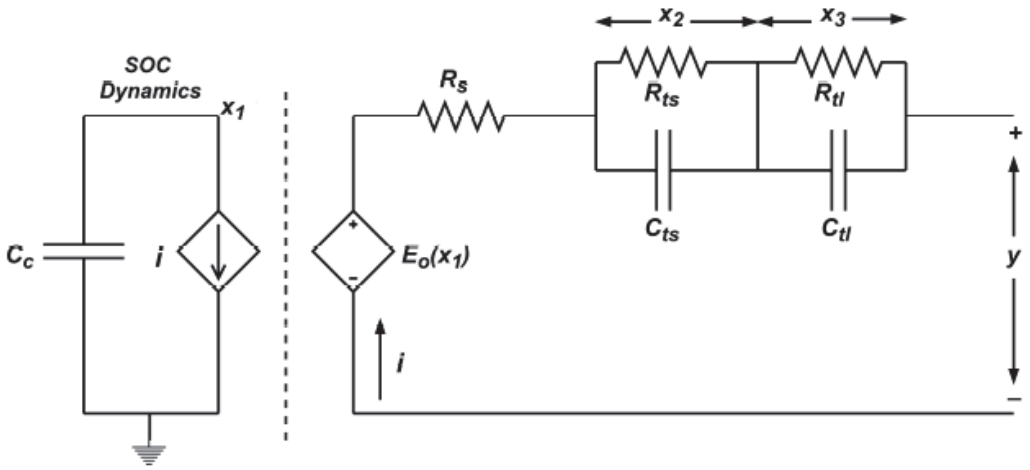

Figure 3.38: Equivalent circuit model for Li-ion battery [42].

$$E_0\,(x_1) = -p_1 e^{-p_2 x_1(t)} + p_3 + p_4 x_1(t) - p_5 x_1^2(t) + p_6 x_1^3(t) \quad (3.\ 47)$$

$$R_{ts}\,(x_1(t)) = p_7 e^{-p_8 x_1(t)} + p_9 \quad (3.\ 48)$$

$$R_{tl}\,(x_1(t)) = p_{10} e^{-p_{11} x_1(t)} + p_{12} \quad (3.\ 49)$$

$$C_{ts}\,(x_1(t)) = -p_{13} e^{-p_{14} x_1(t)} + p_{15} \quad (3.\ 50)$$

$$C_{tl}\,(x_1(t)) = -p_{16} e^{-p_{17} x_1(t)} + p_{18} \quad (3.\ 51)$$

$$R_s\,(x_1(t)) = p_{19} e^{-p_{20} x_1(t)} + p_{21} \quad (3.\ 52)$$

3.11.2. Parameters estimation. A major part of the research field of Li-ion battery model is estimating the parameters p_1 to p_{21} through simulations and experiments, for different batteries with different ratings. The literature review clearly showed the range of ratings currently used in EVs. The voltages used are ranging from 300 V to 450 V, with Ampere hour ratings ranging from 160 to 250 Ah. Accordingly, the estimated parameters for the 400 V battery model, shown in Table 3.7, will be used.

3.11.3. Li-ion battery model simulation. More research into that area resulted in a Simulink model [43] corresponding to the equivalent circuit provided earlier. Figure 3.39 shows the Simulink battery model, where equations (3.47) till (3.52) are embedded inside the blocks corresponding to the voltage source E_0, the resistances R_s, R_{ts}, and R_{tl}, as well as the capacitances C_{ts} and C_{tl}, which are found inside the

subsystems named as “SOC” and “Battery Model”. Moreover, a simple modification was done to adjust the battery’s Ampere hour to 225 Ah, which matches an average EV’s battery rating. A 225 Ah battery would last for 225 hours if discharged from 100% to 0% SOC, at a rate of 1 A. This translates into 810000 seconds. However, the simulation time was decreased to 790000 seconds to avoid the very last discharge part, where a sharp voltage drop occurs, which would cause some mathematical computational issues such as an undefined solution. However, the simulation time was decreased to 790000 seconds to avoid the very last discharging part, where a sharp voltage drop occurs, which would cause some mathematical computation issues such as undefined solution.

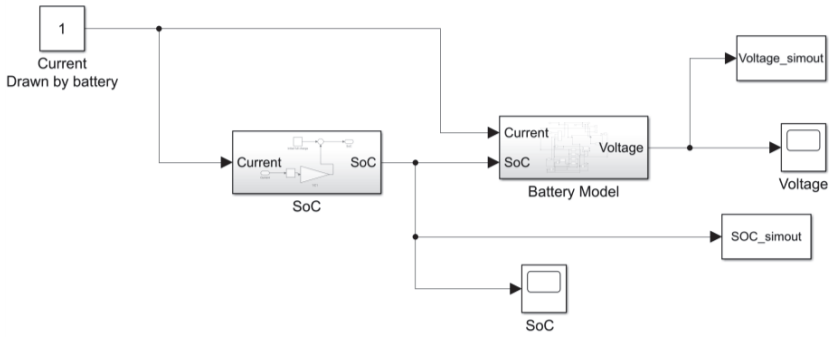

Figure 3.39: Simulink Li-ion battery model [43]

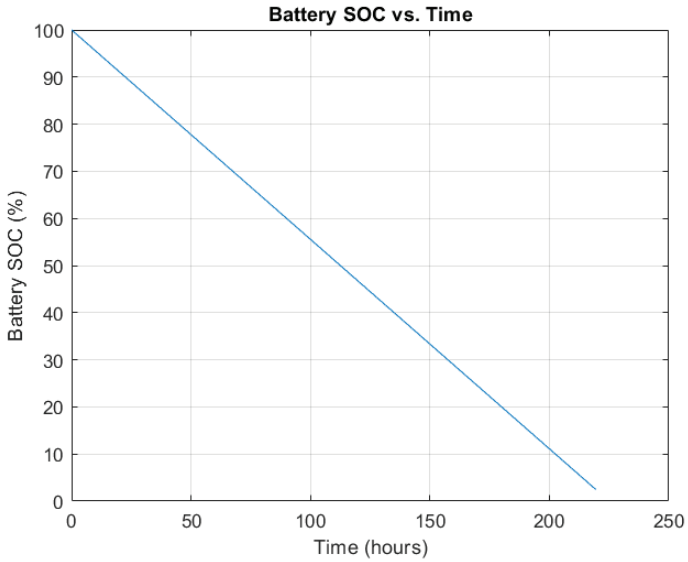

Figure 3.40: Battery’s SOC vs. Time.

Table 3.7: Parameters for a 400 V Li-ion battery bank [42].

Parameter	Estimated value
p_1	97.51
p_2	35.01
p_3	357.236
p_4	5.2
p_5	11.01
p_6	37.55
p_7	0.5643
p_8	30.01
p_9	0.069
p_{10}	6.262
p_{11}	150
p_{12}	0.0693
p_{13}	760.882
p_{14}	10.845
p_{15}	684.626
p_{16}	6000
p_{17}	27.514
p_{18}	3666.71
p_{19}	15.014
p_{20}	27.514
p_{21}	5.428

Table 3.8: Battery's voltage and equivalent impedance at different values of SOC.

SOC	Voltage (V)	Z_{eq} (nΩ)
1	388.9760	5.4280e+09 - 2.7602i
0.9	380.3718	5.4280e+09 - 2.7603i
0.8	373.5752	5.4280e+09 - 2.7606i
0.7	368.3607	5.4280e+09 - 2.7615i
0.6	364.5032	5.4280e+09 - 2.7640i
0.5	361.7772	5.4280e+09 - 2.7716i
0.4	359.9575	5.4282e+09 - 2.7944i
0.3	358.8163	5.4319e+09 - 2.8647i
0.2	358.0473	5.4892e+09 - 3.1015i
0.1	354.7418	6.3865e+09 - 4.2107i

The reason why the Simulink model was used here, is to validate the estimated parameters, and observe the relations between the battery's SOC, voltage, and time. Figures 3.40, 3.41, and 3.42 show the battery's SOC versus time, the battery's voltage versus time, and the battery's voltage versus its SOC, respectively. A code was also written to calculate the battery's voltage E_0 and the equivalent battery impedance,

which consists of R_s in series with R_{ts} paralleled with C_{ts}, and R_{tl} paralleled with C_{tl}. The results are tabulated as shown in Table 3.8.

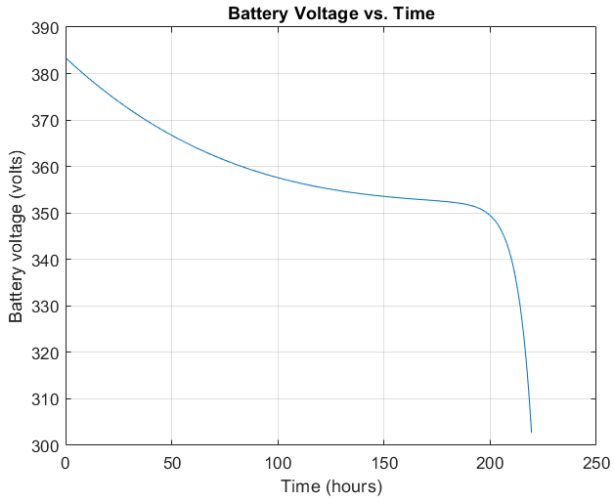

Figure 3.41: Battery's voltage vs. Time.

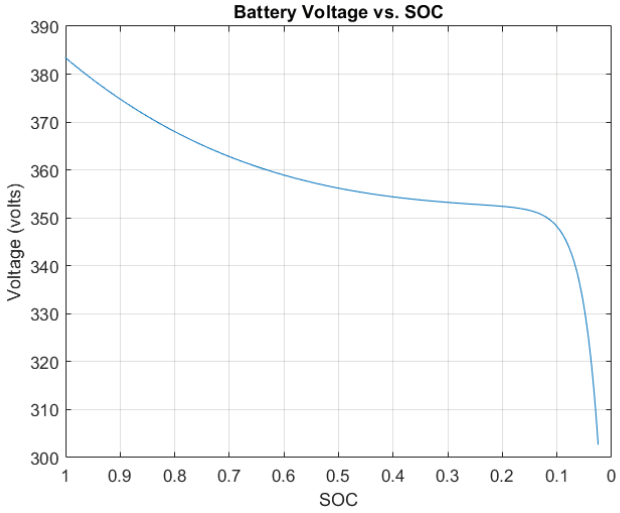

Figure 3.42: Battery's voltage vs. Battery's SOC.

Chapter 4. Results

This chapter will list down the final results obtained from this research. The results are mainly obtained from simulations done on ANSYS Maxwell and ANSYS Simplorer. The designs done on those two software were aided by the optimization done earlier using MATLAB besides analytical optimization. The following flowchart briefs the chapter's topics.

4.1. ANSYS Maxwell Simulation Outcomes

The main outcomes of Maxwell simulation can be briefed as follows:

- Coupling coefficient between the transmitting and receiving coils at different separating distances
- Transmitter's inductance at different separating distances
- Receiver's inductance at different separating distances
- Field plot between the two coils as shown in Figure 4.1

Figure 4.1: Simulation of WPT taking place between the transmitter coil embedded underground, and the receiver coil fixed at the bottom of the car.

Nine ANSYS Maxwell simulation samples were run to get the coupling coefficient, transmitter's self-inductance, and receiver's self-inductance for each of the 9 case studies. Table 4.1 shows the results obtained. Figures 4.2 till 4.10 shows the field plots for case studies 1 till 9, respectively. All simulations were done at a separation distance (h) of 90mm.

Table 4.1: ANSYS Maxwell results.

Case scenario	Misalig. (%)	Rec. CHR	Transm. CHR	Coupling coefficient	Transm. self-inductance (μH)	Rec. self-inductance (μH)
1	0	const.	const.	0.552	36.193	29.746
2	10	const.	const.	0.544	28.43	38.17
3	20	const.	const.	0.519	28.41	38.17
4	0	variable	variable	0.516	15.09	15.29
5	10	variable	variable	0.504	15.09	15.29
6	20	variable	variable	0.434	12.644	13.089
7	0	variable	const.	0.497	12.645	38.174
8	10	variable	const.	0.492	12.646	38.174
9	20	variable	const.	0.473	12.642	38.174

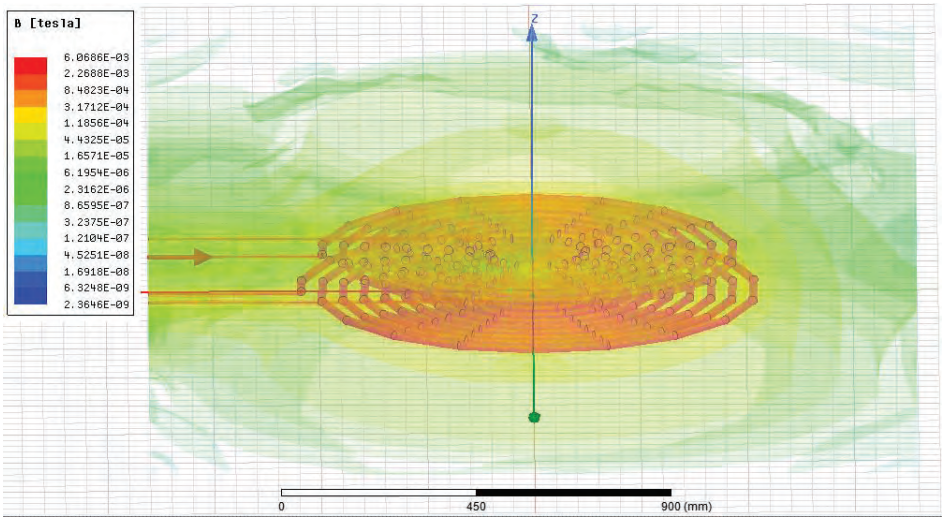

Figure 4.2: Field plot for case study 1 using ANSYS Maxwell simulation.

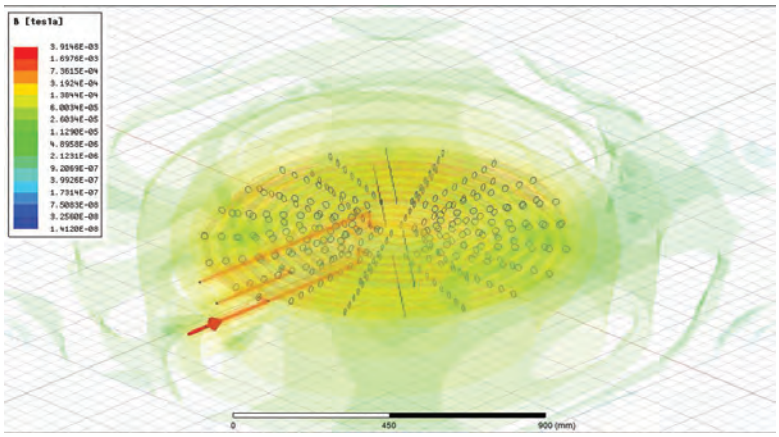

Figure 4.3: Field plot for case study 2.

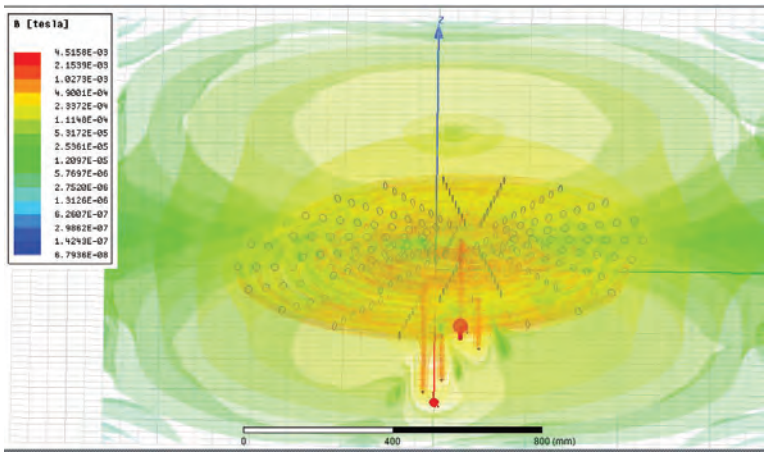

Figure 4.4: Field plot for case study 3.

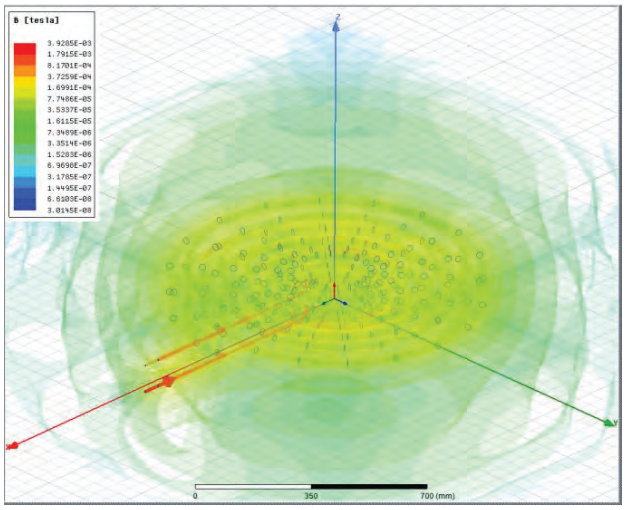

Figure 4.5: Field plot for case study 4.

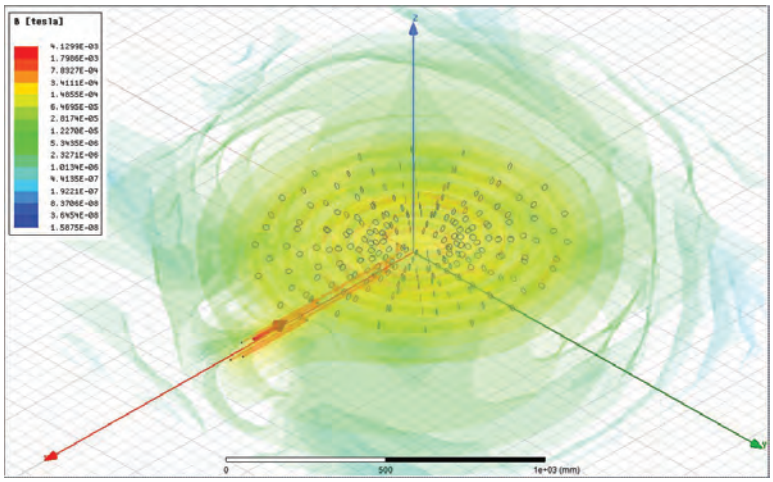

Figure 4.6: Field plot for case study 5.

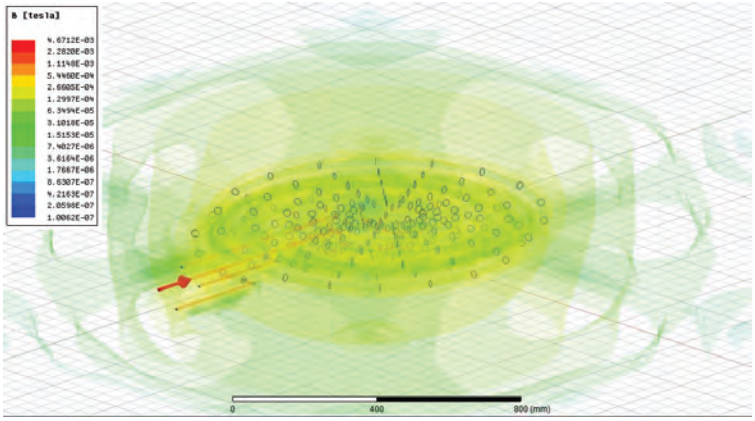

Figure 4.7: Field plot for case study 6.

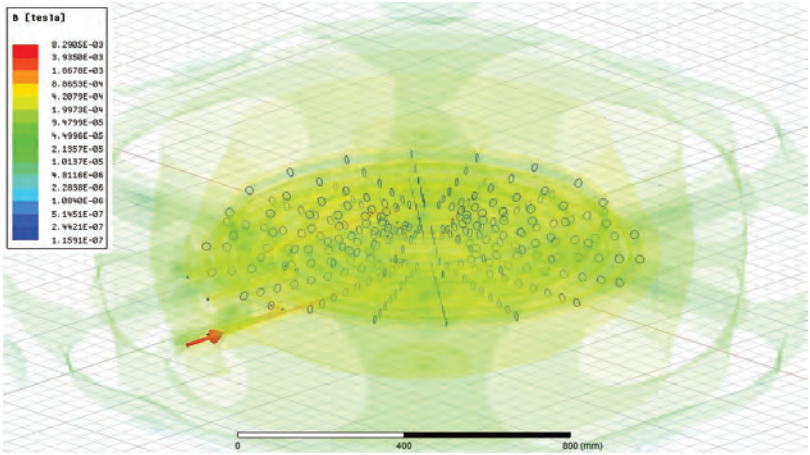

Figure 4.8: Field plot for case study 7.

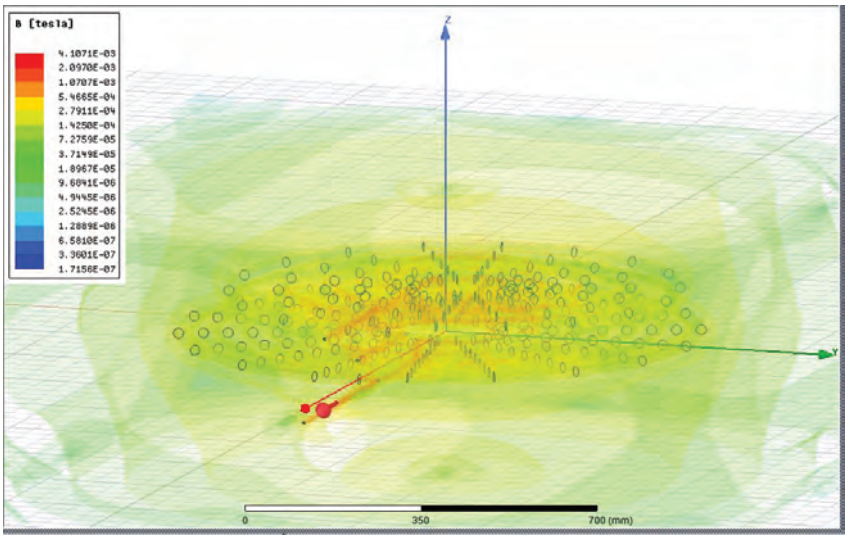

Figure 4.9: Field plot for case study 8.

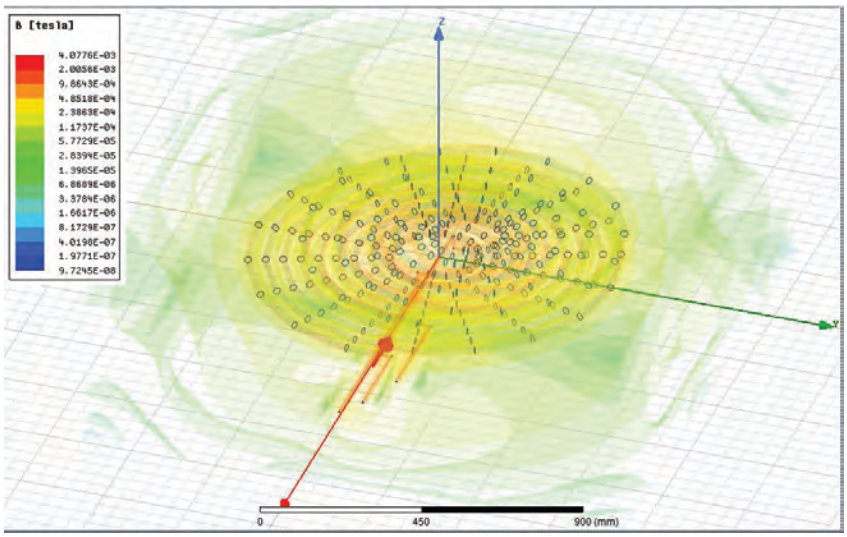

Figure 4.10: Field plot for case study 9.

The outcomes of ANSYS Maxwell simulation for the case study of double receivers came out to be less desirable than the case of single receiver. The coupling coefficient was around 20% less than the average of single receiver case studies. Furthermore the transmitted power dropped by around 15% compared to the average single receiver case studies.

4.2. ANSYS Simplorer Simulation Outcomes

In this section, Simplorer simulations outcomes will be shown and discussed. The coils designed on Maxwell for different case studies, were inserted into the circuit designed on Simplorer, shown in Figure 3.37. Primary and secondary sides' capacitors were chosen using equation (3.40), depending on the inductance values of the transmitting and receiving coils, in addition to the chosen resonance frequency, which was picked to be 100 kHz in this research. The AC voltage source was set at an amplitude of 326V. That is an RMS value of 230 V, similar to the usual low voltage level. As noticed, the full system is a combination of electrical and magnetic components. ANSYS Simplorer provides the capability of solving electrical and magnetic fields simultaneously.

4.2.1. Efficiency of no misalignment and constant change in radius. Through the outcomes obtained in Table 3.1, the capacitors on the transmitter and receiver sides were calculated for each case study. The calculated values cause the entire circuit to resonate at the same frequency, providing maximum efficiency of power transfer. Figure 4.11 shows a couple of informative outcomes. The first is the resonance, occurring at 140.25 kHz as indicated by marker m2, which corresponds to the power efficiency plot in red. As discussed in section 3.9.3, the shift in resonance frequency occurs due to the magnetic inductance. The second point to look at is the amount of power received, which is plotted in green. Marker m1 indicates that at 140.25 kHz, the power received by the battery reaches 17.41 kW.

4.2.2. Efficiency of 10% misalignment and constant change in radius. The outcomes obtained when simulating case study 2 are shown in Figure 4.12. Resonance occurred at 139.15 kHz, with 17.34 kW received by the battery for charging. It can be seen that due to the variable change in radius in both coils, their self inductance changed, and therefore magnetic inductance changed. This is the reason why resonance shifted by 1.1 kHz from the previous case.

4.2.3. Efficiency of 20% misalignment and constant change in radius. The outcomes obtained when simulating case study 3 are shown in Figure 4.13. Resonance occurred at 136.4 kHz, with 17.06 kW received by the battery for charging.

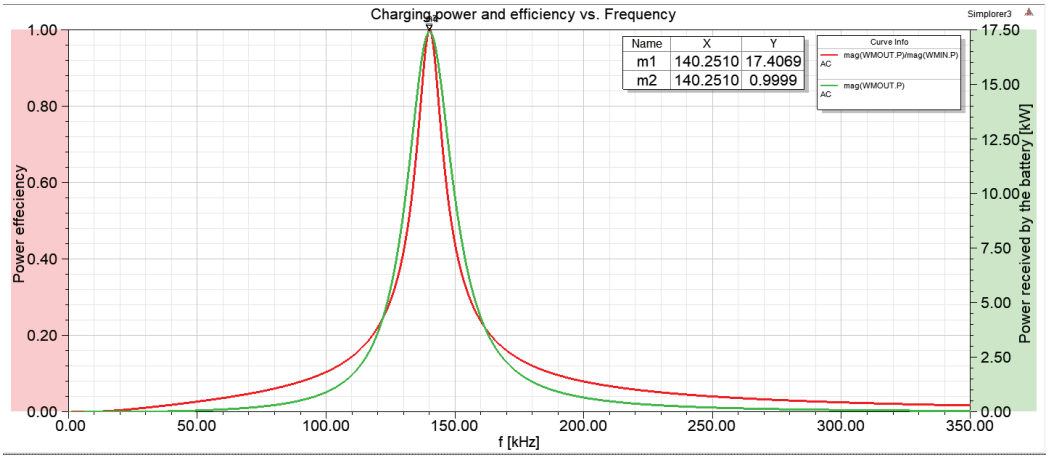

Figure 4.11: ANSYS Simplorer outcomes for case study 1.

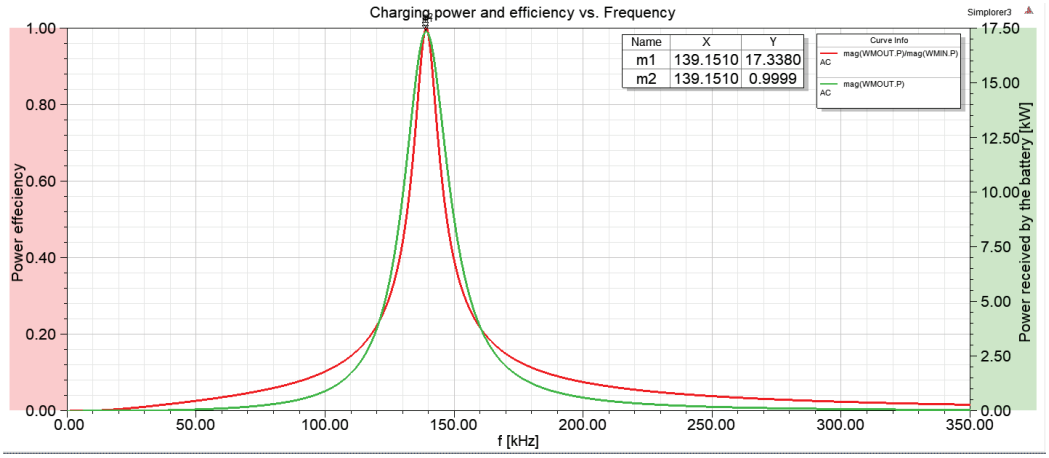

Figure 4.12: ANSYS Simplorer outcomes for case study 2.

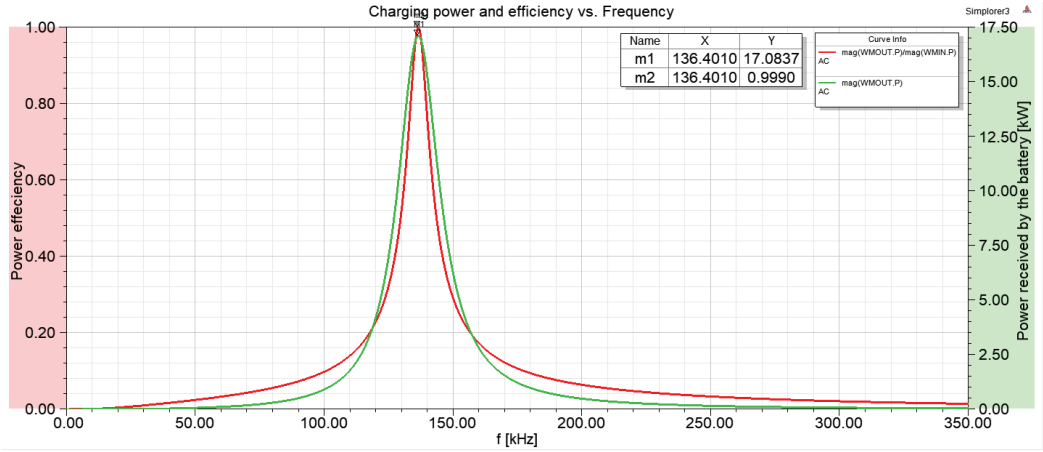

Figure 4.13: ANSYS Simplorer outcomes for case study 3.

4.2.4. Efficiency of no misalignment and variable change in radius in both coils. The outcomes obtained when simulating case study 4 are shown in Figure 4.14. Resonance occurred at 115.5 kHz, with 17.54 kW received by the battery for charging.

4.2.5. Efficiency of 10% misalignment and variable change in radius in both coils. The outcomes obtained when simulating case study 5 are shown in Figure 4.15. Resonance occurred at 114.4 kHz, with 17.44 kW received by the battery for charging.

4.2.6. Efficiency of 20% misalignment and variable change in radius in both coils. The outcomes obtained when simulating case study 6 are shown in Figure 4.16. Resonance occurred at 112.2 kHz, with 17.1 kW received by the battery for charging.

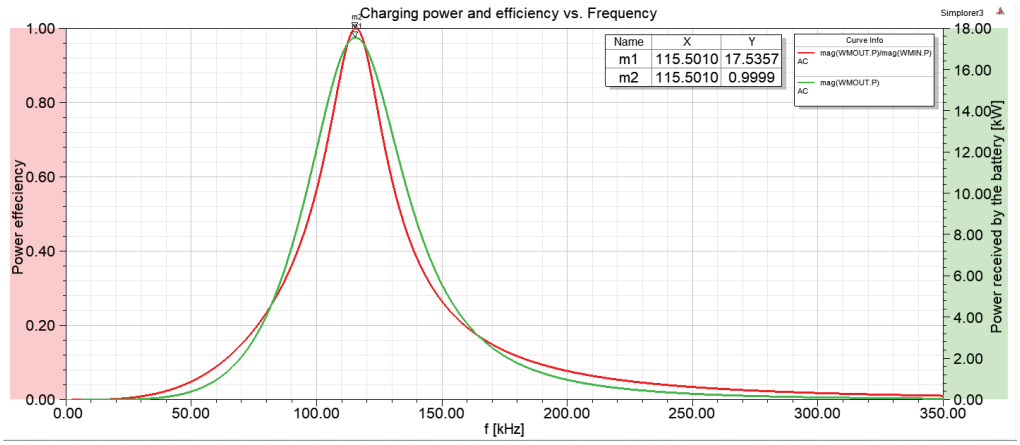

Figure 4.14: ANSYS Simplorer outcomes for case study 4.

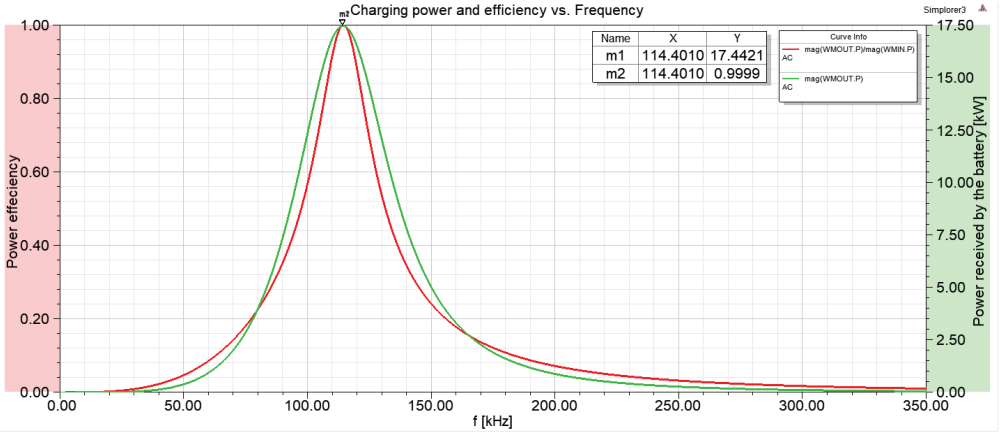

Figure 4.15: ANSYS Simplorer outcomes for case study 5.

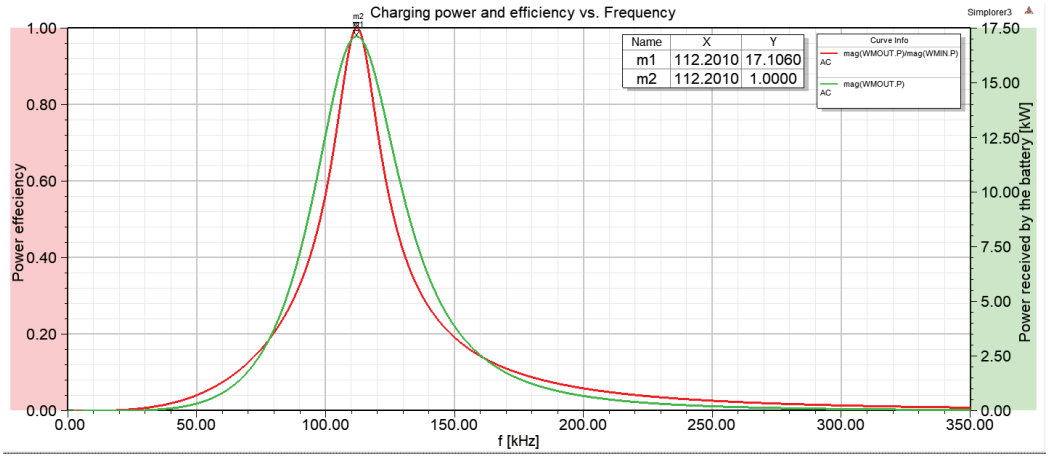

Figure 4.16: ANSYS Simplorer outcomes for case study 6.

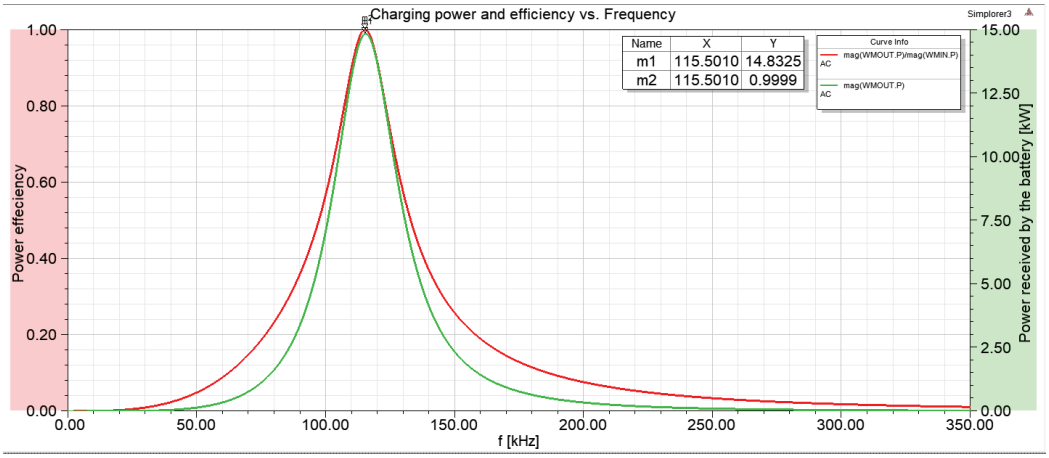

Figure 4.17: ANSYS Simplorer outcomes for case study 7.

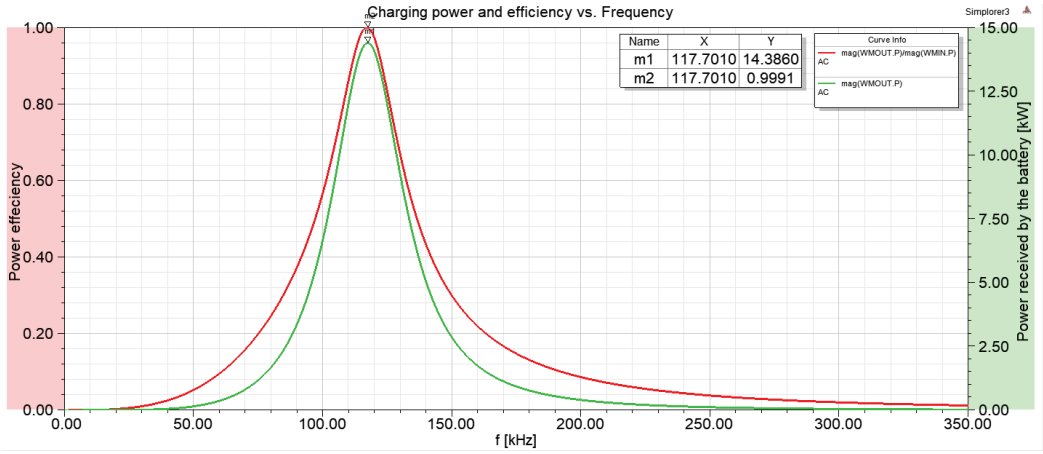

Figure 4.18: ANSYS Simplorer outcomes for case study 8.

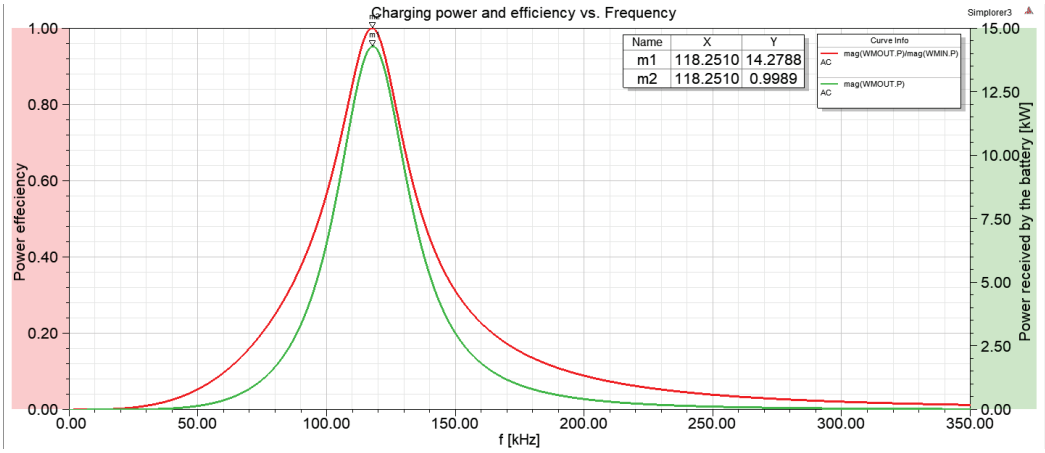

Figure 4.19: ANSYS Simplorer outcomes for case study 9.

4.2.7. Efficiency of no misalignment and variable change in radius in receiver coil. The outcomes obtained when simulating case study 7 are shown in Figure 4.17. Resonance occurred at 115.5 kHz, with 14.83 kW received by the battery for charging.

4.2.8. Efficiency of 10% misalignment and variable change in radius in receiver coil. The outcomes obtained when simulating case study 8 are shown in Figure 4.18. Resonance occurred at 117.15 kHz, with 14.4 kW received by the battery for charging.

4.2.9. Efficiency of 20% misalignment and variable change in radius in receiver coil. The outcomes obtained when simulating case study 9 are shown in Figure 4.19. Resonance occurred at 118.25 kHz, with 14.28 kW received by the battery for charging.

4.3. Coils Weights and Material Volume

It's indeed important to look into how much material is being used to construct both coils. As for the transmitter coil, the weight isn't an essential factor to look into as the coil will be embedded underground. However, the amount of material being used greatly affects the price. On the other hand, the weight of the receiver coil can be a factor of importance as it will affect the total weight of the electric vehicle, which has an effect on the total power consumption of the EV. Moreover, the amount of material being used, or in other words the material's volume, affects the price of the coil. This

part studies the weights and volumes of all coils used in the previously mentioned case studies. Equation (3.12) was used to calculate the lengths of the coils, which is then used to get the material's volume. Equation (3.14) gives the coil weight, with copper used as the coil material.

4.3.1. Coil weight and volume in cases of a constant change in radius. Plugging in the values of starting radius, change in radius, and number of turns into equation (3.12) yielded to a coil having a wire length of 15 meters. Since the used wire radius is 1 cm, therefore the volume of the material used is 4712 cm^3. In this case, when using copper, the receiving coil weight would be 42 kg.

4.3.2. Coil weight and volume in cases of a variable change in radius. As for the case of having a variable change in radius, the designed coil had 6 turns divided into 3 couples. The change in radius was variable among the 3 couples, starting at 4 cm, moving to 7 cm, and ending at 10 cm. The starting radius of the coil was 8 cm, therefore the starting radius of the inner couple of turns was taken as 8 cm. The middle couple of turns consequently had a starting radius of 16 cm, and 30 cm for the last couple of turns. The earlier mentioned calculations yielded to a receiver coil of a total wire length of 9.43 meters, material volume of 2964 cm^3, and a weight of 26.5 kg.

The idea of having a variable change in radius resulted in a reduction of 15.5 kg in the coil weight, that's 37% of the initial coil weight. Furthermore, the amount of copper used dropped from 4712 cm^3 to 2964 cm^3, that's again 37% reduction in the material used, which can translate into a recognizable reduction in the coils' manufacturing cost and selling price.

4.4. Results Tabulation and Comparison

This section will tabulate all the results obtained from the simulations done on ANSYS, using different case scenarios. Table 4.2 shows 9 case scenarios, divided into 3 main categories, with their different geometrical properties with respect to misalignment and change in radius (CHR), in addition to the coils' weights. The actual resonance frequencies are listed, in addition to the amount of power delivered to the EV's battery. It is clear that category B resulted in the most desirable outputs, where the power received by the battery is maximum when compared to other categories, and the coils' weights are minimum. This shows that having a variable change in radius in

Table 4.2: ANSYS results.

Category	Case	Misalig. (%)	Rec. CHR	Transm. CHR	Rec. weight (kg)	Transm. weight (kg)	Resonance freq. (Hz)	$P_{received}$ (kW)
	1	0	const.	const.			140.25	17.41
A	2	10	const.	const.	42	42	139.15	17.34
	3	20	const.	const.			136.40	17.06
	4	0	variable	variable			115.50	17.54
B	5	10	variable	variable	26.5	26.5	114.40	17.44
	6	20	variable	variable			112.20	17.10
	7	0	variable	const.			115.50	14.83
C	8	10	variable	const.	26.5	42	117.15	14.40
	9	20	variable	const.			118.25	14.28

both the transmitter and receiver coils optimizes the system, with respect to power efficiency and coils weights and prices.

4.5. Wireless Charging Time

This section discusses the time needed to wirelessly charge different EVs using category B coil design. Different EVs battery ratings were shown in Table 2.1. Accordingly, a Toyota Prius can be fully charged from zero in 15 minutes, a Chevy Volt or a Mitsubishi iMiEV needs 55 minutes, a BMW i3 needs an hour and 15 minutes, while a Nissan Leaf needs an hour and 40 minutes. Section 2.5 mentions that BMW 530e iPerformance model can be fully reloaded in three and a half hours using its wireless charger. The optimized category B coil design shown in this thesis would decrease the charging time of a BMW 530e iPerformance to 2 hours and 10 minutes.

4.6. Comparison Between Different Coil Designs With Respect to the Consumed Power

Equation (3.46) was used to calculate the EV's consumed power before adding the receiving coil, and after adding different designs of receiving coils. For an average electric vehicle, the mass without installing the receiving coil is approximately 2000 kg. The average frontal area A_F is 2.77 m^2, the acceleration from 0 to 100 km/h takes around 6 seconds, and the coefficient of drag C_D is around 0.3. The average velocity

will be taken as 75 km/h, the grade angle α will be taken as zero, and the rolling resistance coefficient is taken as 0.02 s^2/m^2. Calculating the consumed power before and after installing the receiving coil with variable change in radius, having a weight of 26.5 kg, shows that the coil weight only increased the amount of consumed power by 1.32%. On the other hand, when using a receiving coil having a constant change in radius, not only it is most expensive due to the 37% extra material used, but it also consumes 2.1% more power due to its weight.

4.7. Relation Between Battery's SOC and the Resonance Frequency

The data obtained in Table 3.8 was used to check the effect of the change in the battery's SOC, and thus the possible change in the battery's internal impedance, on the resonance frequency and the WPT efficiency.

The case study of perfect alignment and variable change in radius in receiver coil was used to test the effect of the change in SOC on the resonance frequency and the transmitted power. The same Simplorer model shown in Figure 3.37 was used to simulate the WPT process. The simulation was run 10 times, for 10 different values of battery SOC. At each run of simulation, the battery's voltage, inner resistance, and inner capacitance were adjusted according to the data shown in Table 3.8. The results showed that the resonance frequency and transferred power remained constant when the SOC varied from 1 to 0.2, where 14.27 kW where transferred at 118.25 kHz, as shown in Figure 4.20. However, at SOC value of 0.1, where the sudden drop in voltage occurs, the resonance frequency shifted by 1.1 kHz to become 119.35 kHz. Moreover, the transferred power dropped by 0.87 kW to become 13.4 kW, as shown in Figure 4.21.

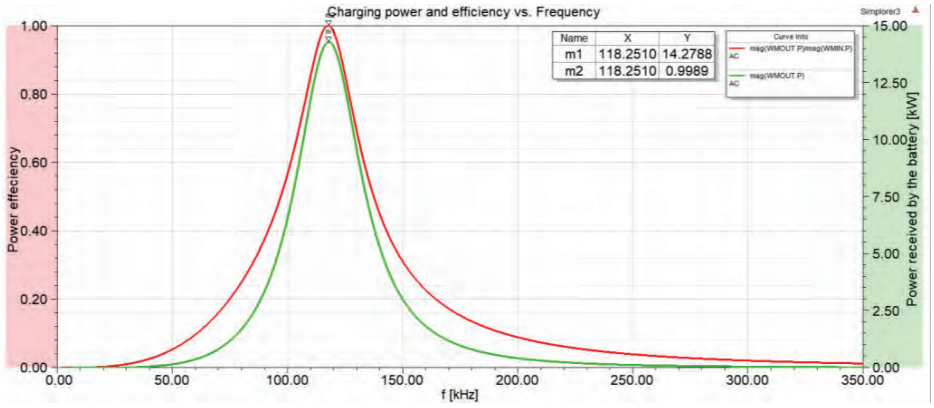

Figure 4.20: Power transferred with battery SOC varying from 1 to 0.2.

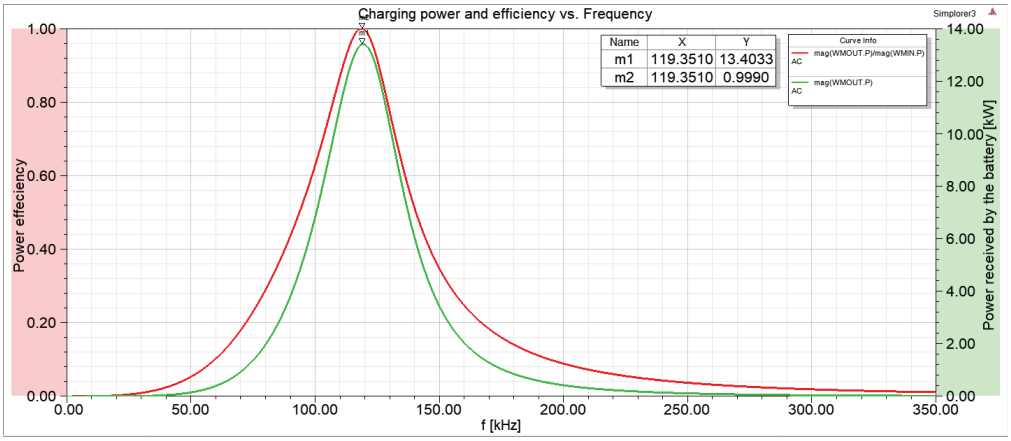

Figure 4.21: Power transferred with a battery SOC of 0.1.

As noticed, the changes in the resonance frequency at different SOCs are negligible. Therefore the WPT coils are expected to deliver maximum power throughout the entire charging process, if it is set to operate at resonance.

4.8. Current Delivered to the EV's Battery During Charging

It was necessary to check the maximum value of current delivered to the EV's battery during charging, and make sure it is in the allowable range. It was found through Simplorer simulations that the maximum charging current at resonance is 56.8A, as shown in Figure 4.22. Literature review shown in chapter 2 shows that the average chargers operate at 30 A, while superchargers, such as the Tesla supercharger, operate at 120 A. Furthermore, BMW are currently working on developing a supercharger that operates at 900 V, 500 A, for a charging rate of 450 KW [44]. This shows that 56.8A is a reasonable range to operate at.

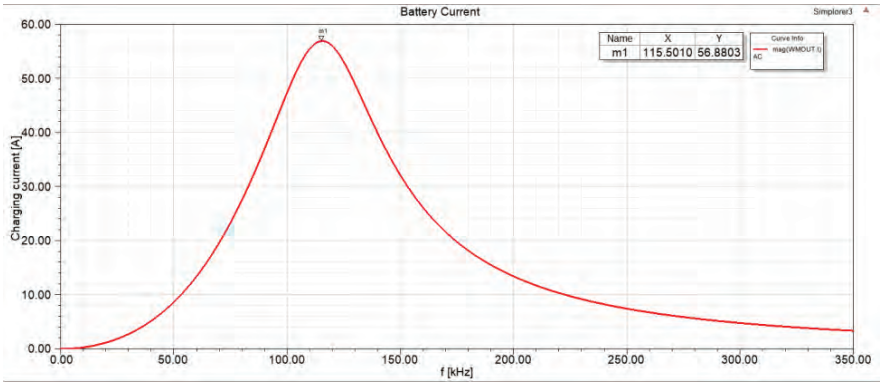

Figure 4.22: Maximum current delivered to the battery during charging.

Chapter 5. Conclusion and Future Work

5.1. Conclusion

This research presents efficient wireless power transfer (WPT) coil designs for EVs wireless charging. The main geometrical perspectives addressed were the change in radius, and the coils diameters. It was clearly shown how the geometry affects the power transfer efficiency, in addition to the coil weight and amount of material used to manufacture it. This can contribute to a significant reduction in the coil price and weight. This research outcomes showed clearly that the maximization and synchronization between the transmitting and receiving coils' diameters result in a higher WPT efficiency. The research also revealed how the usage of variable change in radius is favourable. The idea of having a variable change in radius is considered the main novel contribution in this thesis. The coils used in the final simulations were chosen to have a ratio between the inner turns, middle turns, and outer turns' change in radius of 4:7:10, meaning that if the number of receiver coil turns is 6, and the inner 2 turns have a change in radius of 4 cm, then the middle 2 turns would have a 7 cm change in radius, while the outer 2 turn would have a 10 cm change in radius. The main conclusion of this thesis is that coils of equal diameters and a variable change in radius of 4:7:10 ratio lead to WPT optimization. This ratio was chosen after examining several other ratios, and checking their power transfer behaviour. Having variable change in radius in both the transmitter and receiver coils resulted in the maximum power transfer and the least amount of material used, thus the least cost and weight. The charging time needed to fully charge an EV wirelessly using the optimized coil design was calculated to be an hour and 15 minutes for an average EV.

Optimization of EVs wireless charging would greatly affect the EVs market. Wireless charging technique eliminates any risks of contact wearing or sparks during plugging and unplugging, which is an issue in wired chargers. Wireless charging would be a greatly more convenient charging method if it is made to reach a similar charging speed of wired chargers.

The coils design, electromagnetic simulation, and full circuit analysis of the EV's WPT process, done on ANSYS Maxwell and ANSYS Simplorer, provides informative outcomes and worthwhile data that can be effectively used to improve the

system design. These simulations can also be used for almost zero cost experimenting and testing. These reliable simulation tools can also reduce the design cycle time, besides one of the biggest advantages of simulation tools of increasing the knowledge in the field, and opening new horizons for novel ideas.

One of the most valuable uses of the optimization and simulation done in this research, is their ability of providing ready-to-implement data for both EVs manufacturers and electricity utility companies. As for the first, geometrical information was listed down through analytical optimization, as well as software optimization. These geometrical sets of data were used to design coils on the finite element analysis software, ANSYS. Therefore, EVs manufacturers are provided with ready-to-implement coil designs, with full information about their power efficiencies, volumes, and weights. Secondly, for electricity utility companies, the power transfer efficiency provided for different case studies can be used for setting billing scenarios. In other words, to provide a reasonable tariff for EVs wireless charging, it needs to be fair for both the consumer and the provider, which is usually the electricity utility company. For this sake, the ratio of the amount of power provided by the electricity utility company and the amount of power consumed by the EVs battery, has to be known. Through that, the losses can be predicted and calculated, then included in the charging tariff, in a way that makes it fair for both sides.

5.2. Future Work

This section points out some flourishing ideas that seem to have potential and hopefully bright outcomes, as well as opportunities for improvement in the field of EVs wireless charging. Here are some points which can be considered for the future work:

- Since there is a strong relation between the alignment of the transmitter and receiver coils and the wireless power transfer efficiency, as well as a strong relation between the separation distance between the coils and the WPT efficiency, the idea of having movable coils would be greatly advantageous. Suppose the X-axis and Y-axis to be forming the plane parallel to the ground, while the Z-axis to be perpendicular to the ground. The motion of the receiver or transmitter coil in the Z-axis direction would be responsible for minimizing the separation distance, while the motion in X-axis and Y-axis would be

responsible for having a perfect alignment between the coils. Movable coils would result in having the maximum possible WPT efficiency for EV wireless charging. Z-axis motion can depend on a simple sensor that measures the distance. Since one of the outcomes of this research is that the highest WPT efficiency occurs when both coils have the same diameter, therefore the X-axis and Y-axis motion can simply depend on 2 proximity sensors that align the coil pads. X-axis and Y-axis motion will not need to depend on any electromagnetic measurement or any complicated algorithm.

- Perhaps researching into the materials used in the coils manufacturing, and comparing different materials with respect to the WPT performance and the coils prices, can lead to more optimization in terms of materials.
- Applying proper electrical and mechanical safety to the EV wireless charging system might be necessary. One of the main case studies that should be researched into is the possible occurrence of a car accident while the charging process is ongoing. The deformation that can occur to the coil may cause a sudden short circuit or sparks. In addition, the sudden shock resulting from the accident can affect other electrical components and cause safety hazards.
- Looking into increasing the voltage levels of the entire WPT process is an actively ongoing research field, to which contributions would be tremendously valuable, where there’s a strong relation between the voltage level and the amount of power transferred.
- Dynamic wireless charging simulation would be an extremely beneficial contribution, where if dynamic wireless charging is optimized, it will be a breakthrough, providing continuous charging to EVs as they drive on the way. This can lead to great reduction in battery sizes and prices, as well as multiple times longer driving ranges. The most significant benefit of simulation would be the easiness that comes afterwards, when designing the coils, and when applying new design aspects and ideas, which can optimize the dynamic WPT process.

References

[1] C. Custer, “China’s government wants 5 million electric cars on the roads by 2020,” *Tech in Asia - Connecting Asia's startup ecosystem*. [Online]. Available: https://www.techinasia.com/chinas-government-5-million-electric-cars-roads-2020. [Accessed: 01-Mar-2019].

[2] S. Li and C. C. Mi, "Wireless Power Transfer for Electric Vehicle Applications," *in IEEE Journal of Emerging and Selected Topics in Power Electronics*, vol. 3, no. 1, pp. 4-17, March 2015.

[3] I. Suh and J. Kim, "Electric vehicle on-road dynamic charging system with wireless power transfer technology," *2013 International Electric Machines & Drives Conference*, Chicago, IL, 2013, pp. 234-240.

[4] S. Lukic and Z. Pantic, "Cutting the Cord: Static and Dynamic Inductive Wireless Charging of Electric Vehicles," *in IEEE Electrification Magazine*, vol. 1, no. 1, pp. 57-64, Sept. 2013.

[5] V. Sreedhar, "Plug-In Hybrid Electric Vehicles with Full Performance," 2006 *IEEE Conference on Electric and Hybrid Vehicles*, Pune, 2006, pp. 1-2.

[6] T. Lindeman, “Norway's EV Incentives Have Worked. Now What?” CityLab, 27-Dec-2018. [Online]. Available: https://www.citylab.com/environment/2018/12/norway-electric-vehicle-models-incentives-car-free-oslo/578932/. [Accessed: 01-Mar-2019].

[7] I. Phillips, “Top 18 Electric Car Countries (with Chart),” AvtoWow.com | EV & PHEV Resource. [Online]. Available: https://avtowow.com/countries-by-electric-car-use. [Accessed: 15-Mar-2019].

[8] Huawei Yang, Y. Gao, K. B. Farley, M. Jerue, J. Perry and Z. Tse, "EV usage and city planning of charging station installations," *2015 IEEE Wireless Power Transfer Conference (WPTC)*, Boulder, CO, 2015, pp. 1-4.

[9] K. Gammon, “Futuristic Roads May Make Recharging Electric Cars a Thing of the Past,” NBCNews.com, 01-Jun-2017. [Online]. Available: https://www.nbcnews.com/mach/mach/futuristic-roads-may-make-recharging-electric-cars-thing-past-ncna766456. [Accessed: 09-May-2018].

[10] C. C. Mi, G. Buja, S. Y. Choi and C. T. Rim, "Modern Advances in Wireless Power Transfer Systems for Roadway Powered Electric Vehicles," *in IEEE Transactions on Industrial Electronics*, vol. 63, no. 10, pp. 6533-6545, Oct. 2016.

[11] Edelstein, S. (2018). Sweden Modified Road to Charge Electric Vehicles on the Go. [online] Available at: http://www.thedrive.com/tech/20103/sweden-modified-road-to-charge-electric-vehicles-on-the-go [Accessed 19 Oct. 2018].

[12] Sc Tang, Sy Ron Hui, Hsh Chung, A Low-profile Power Converter Using Printed-circuit Board (PCB) Power Transformer with Ferrite Polymer Composite., vol. 16, no. 4, pp. 493-498, 2001.

[13] "Univ City Hong Kong Files European Patent Application for Planar Inductive Battery Charger." in Global IP News. Electrical Patent News, New Delhi, January 2014.

[14] Covic Hao Hao, Boys, "A Parallel Topology for Inductive Power Transfer Power Supplies", *Power Electronics IEEE Transactions on*, vol. 29, no. 3, pp. 1140-1151, 2014.

[15] M. Budhia, J. T. Boys, G. A. Covic, Chang-Yu Huang, "Development of a Single-sided Flux Magnetic Coupler for Electric Vehicle IPT Charging Systems. (inductively Power Transfer) (Technical Report)", *IEEE Transactions on Industrial Electronics,* vol. 60, no. 1, pp. 318, 2013.

[16] N. A. Keeling, G. A. Covic, J. T. Boys, "A Unity-Power-Factor IPT Pickup for High-Power Applications", *Industrial Electronics IEEE Transactions on,* vol. 57, no. 2, pp. 744-751, 2010.

[17] Michael L G Kissin, Grant A Covic, John T Boys, "Steady-State Flat-Pickup Loading Effects in Polyphase Inductive Power Transfer Systems", *Industrial Electronics IEEE Transactions on,* vol. 58, no. 6, pp. 2274-2282, 2011.

[18] C. -Y. Huang, J. T. Boys, G. A. Covic, "LCL Pickup Circulating Current Controller for Inductive Power Transfer Systems", *IEEE Transactions on Power Electronics*, vol. 28, no. 4, pp. 2081-2093, 2013.

[19] "BMW Group," BMW Group. [Online]. Available: https://www.bmwgroup.com/en.html. [Accessed: 05-Mar-2019].

[20] Evatran, "Wireless charging upgrade now available for Tesla Model S," Plugless Power. [Online]. Available: https://www.pluglesspower.com/shop/reserve-tesla-model-s/. [Accessed: 05-Mar-2019].

[21] M.P. Theodoridis, "Effective capacitive power transfer", *IEEE Transactions on Power Electronics*, vol. 27, no. 12, pp. 4906-4913, 2012.

[22] F. Lu, H. Zhang, H. Hofmann, C. Mi, "A double-sided LCLC-compensated capacitive power transfer system for electric vehicle charging", *IEEE Transactions on Power Electronics*, vol. 30, no. 11, pp. 6011-6014, 2015.

[23] F. Lu, H. Zhang, C. Mi, "A review on the recent development of capacitive wireless power transfer technology", *MDPI Energies*, vol. 10, no. 11, pp. 1752, 2017.

[24] A. Kurs, A. Karalis, R. Moffatt, J.D. Joannopoulos, P. Fisher, M. Soljacic, "Wireless power transfer via strongly coupled magnetic resonances", *Science*, vol. 317, no. 5834, pp. 83-86, 2007.

[25] K. Aditya, S.S. Williamson, "Design considerations for loosely coupled inductive power transfer (IPT) system for electric vehicle battery charging—A comprehensive review", *IEEE Transportation Electrification Conference and Expo (ITEC)*, pp. 1-6, 2014.

[26] R. Bosshard, J.W. Kolar, "Inductive power transfer for electric vehicle charging: Technical challenges and tradeoffs", *IEEE Power Electronics Magazine*, vol. 3, no. 3, pp. 22-30, 2016.

[27] Jerram, l. (2018). What's the current state of wireless EV charging? [online]. Available at: https://chargedevs.com/features/whathttps://chargedevs.com/features/whats-the-current-state-of-wireless-ev-charging/s-the-current-state-of-wireless-ev-charging/ [Accessed 29 Oct. 2018].

[28] S. Jeong, Y. J. Jang and D. Kum, "Economic Analysis of the Dynamic Charging Electric Vehicle," *in IEEE Transactions on Power Electronics*, vol. 30, no. 11, pp. 6368-6377, Nov. 2015.

[29] Jelic, L. (2017). Qualcomm demonstrates dynamic wireless vehicle charging. [online] TweakTown. Available at: https://www.tweaktown.com/news/57646/qualcomm-demonstrates-dynamic-wireless-vehicle-charging/index.html [Accessed 10 Oct. 2018].

[30] L. Shuguang, Y. Zhenxing and L. Wenbin, "Design and Simulation of Coupling Coil for EV's Wireless Charging System*," 2018 IEEE International Conference on Electronics and Communication Engineering (ICECE)*, Xi'an, China, 2018, pp. 115-119.

[31] L. Tan, S. Pan, X. Huang, and C. Xu, "System optimization for wireless power transfer system with double transmitters," *2017 IEEE PELS Workshop on Emerging Technologies: Wireless Power Transfer (WoW)*, 2017.

[32] J. Song, M. Liu, and C. Ma, "Efficiency optimization and power distribution design of a megahertz multi-receiver wireless power transfer system," *2017 IEEE PELS Workshop on Emerging Technologies: Wireless Power Transfer (WoW)*, 2017.

[33] S. Li and C. C. Mi, "Wireless Power Transfer for Electric Vehicle Applications," *in IEEE Journal of Emerging and Selected Topics in Power Electronics*, vol. 3, no. 1, pp. 4-17, March 2015.

[34] L. Shuguang, Y. Zhenxing and L. Wenbin, "Design and Simulation of Coupling Coil for EV's Wireless Charging System," *2018 IEEE International Conference on Electronics and Communication Engineering (ICECE)*, Xi'an, China, 2018, pp. 115-119.

[35] M. Alatalo, E. Palmberg, S. T. Lundmark, T. Thiringer, and R. Karlsson, "Wireless charging for vehicles-some key elements," *2014 16th European Conference on Power Electronics and Applications*, 2014.

[36] J. Liu, Y. Zhang, Z. Wang and M. Cheng, "Design of a High-Efficiency Wireless Charging System for Electric Vehicle," *2018 1st Workshop on Wide Bandgap Power Devices and Applications in Asia (WiPDA Asia)*, Xi'an, China, 2018, pp. 40-44.

[37] L. Bian, Y. Wen, P. Li, Y. Wu, X. Zhang, and M. Li, "Magnetostrictive stress induced frequency shift in resonator for magnetic field sensor," *Sensors and Actuators A: Physical*, vol. 247, pp. 453–458, 2016.

[38] R. Yan, X. Guo, S. Cao, and C. Zhang, "Optimization of output power and transmission efficiency of magnetically coupled resonance wireless power transfer system," *AIP Advances*, vol. 8, no. 5, p. 056625, 2018.

[39] A. Agcal, S. Ozcira and N. Bekiroglu (June 29th 2016). Wireless Power Transfer by Using Magnetically Coupled Resonators, Wireless Power Transfer - Fundamentals and Technologies, Eugen Coca, IntechOpen, DOI: 10.5772/64031. Available from: https://www.intechopen.com/books/wireless-power-transfer-fundamentals-and-technologies/wireless-power-transfer-by-using-magnetically-coupled-resonators

[40] R. Feng, N. Roscoe, L. Qaseer, M. Bojarski, J. Shin, D. Czarkowski, F. D. Leon, S. Finney, and Q. Deng, "Magnetic field distribution in a WPT system for electric vehicle charging," *2016 Progress in Electromagnetic Research Symposium (PIERS)*, 2016.

[41] A. Gupta and V. Bhise, "Relationship of customer needs to electric vehicle performance," *2009 IEEE Vehicle Power and Propulsion Conference*, Dearborn, MI, 2009, pp. 46-52.

[42] H. M. U. Butt, “Real Time Li-ion Battery Bank Parameters Estimation for Electric Vehicle Traction System,” M.S. thesis, College of Engineering, Department of Electrical Engineering, American University of Sharjah, Sharjah, 2019. Accessed on: September 16, 2019. [Online]. Available: https://dspace.aus.edu:8443/xmlui/handle/11073/16439

[43] H. M. Usman, S. Mukhopadhyay, and H. Rehman, “Universal Adaptive Stabilizer Based Optimization for Li-Ion Battery Model Parameters Estimation: An Experimental Study,” IEEE Access, vol. 6, pp. 49546–49562, 2018.

[44] F. Lambert, “BMW and Porsche join forces to enable 15-min electric car charging at 450 kW charge rate,” Electrek, 05-Dec-2017. [Online]. Available: https://electrek.co/2017/12/05/bmw-porsche-electric-car-charging-450-kw-charge-rate/. [Accessed: 01-Nov-2019].

Vita

Abdalla Gesrou was born in 1993, in Abu Dhabi, United Arab Emirates. He received his primary education in Abu Dhabi, UAE, before moving to Alexandria, Egypt, where he did his secondary education and graduated from high school with a score exceeding 100%. He received his B.Sc. degree in Electrical Power Engineering with Honor’s grade from Alexandria University in 2017.

In January 2018, he joined the Mechatronics Engineering master's program in the American University of Sharjah as a graduate teaching assistant. His research interest is in electric vehicles’ wireless charging.